Calculation and Comparison of Propeller Unsteady Pressure Forces on Ships

W. S. Vorus, Associate Member, University of Michigan
Ann Arbor, Michigan

J. P. Breslin, Member, Stevens Institute of Technology,
Hoboken, New Jersey

Y. S. Tein, Associate Member, American Bureau of Shipping,
New York, New York

ABSTRACT

    A formula previously developed for calculating propeller-induced vibratory hull surface forces is reorganized for improved computational efficiency. The reorganized formula is simplified to several alternative forms which are more readily usable by the designer. Specifically, for non-cavitating conditions, a simple relation is derived by which the vertical hull surface force can be estimated if the propeller bearing forces are known. Data which pertains to the stern surface shape is required in the formula; this data for sterns representing the two characteristically different types is included in the paper. Two simplified formulas for estimation of hull surface forces associated with cavitation are also derived. The accuracy of the several simplified formula proposed is judged on the basis of more rigorous computations performed on four different ships.

NOMENCLATURE

A_e	= expanded area of propeller
$\dot{A}_m$	= m^{th} harmonic of time variation of cavity cross-sectional area
a_{ms}, b_{ms}	= coefficients in Legendre function expansion
A_o	= propeller disk area
$B(r_1, \alpha)$	= surface area of propeller blade
$C(x_o)$	= contour of hull section at station x_o
C_{jk}	= influence coefficient in hull surface source density computation
D	= propeller diameter
d	= local draft of hull in vertical plane of propeller
$\vec{e}_r, \vec{e}_\theta$	= unit vectors in radial and tangential directions in propeller disk
EXT	= maximum angular extent of propeller blade cavitation

$F(\zeta)$	= complex potential of flat strip
F_{in}	= amplitude of nth blade rate harmonic of hull surface force in direction i
F_{vbn}^{-}, F_{vbn}^{+}	= $nN{\pm}1$ components of nth blade rate harmonic vertical bearing force
F_{3n}^{c}, F_{3n}^{nc}	= amplitudes of cavitating and non-cavitating vertical hull surface forces
G	= infinite fluid Green's function
G_ν	= ν^{th} harmonic of G in propeller disk
H_{in}	= amplitude of bare hull vibratory velocity potential
H_{jk}	= kernel of hull contour source density equations
i	= subscript defining direction of excitation force; also $\sqrt{-1}$
$\vec{i}$	= unit vector in axial direction
I^ν	= hull section contour integral
j	= index on hull section contour line segments
J	= number of hull section contour line segments per quadrant
k	= index on hull section contour control points; also propeller blade index
K_i	= function related to hull surface source distribution
$\vec{K}_m$	= vector representing m^{th} harmonic propeller blade loading and thickness
ℓ	= half-width of infinite strip; also semi-beam of hull in propeller plane; also length along propeller blade section; also length along hull section contour

L_f, L_a = distances to forward and aft ends of ship in hull coordinate system

$\vec{L}_m$ = vector representing mth propeller blade loading harmonic

LE = propeller section leading edge

m = subscript denoting harmonic order; also abbreviation for meters

M = number of axial stations over length of hull

n = blade rate harmonic order; also index on hull stations

$\vec{n}$ = unit normal vector on hull surface

$\vec{n}_p$ = unit normal vector on propeller blade pitch surface

N = number of propeller blades

$\vec{N}_j$ = unit normal on hull section segmented contour

P = control point in hull surface source density computation

$P(r_1)$ = propeller pitch distribution

$P(\vec{R}_1)$ = propeller blade surfaces

q = propeller blade source distribution

Q = source point in hull surface source density computation

$Q_{\nu-1/2}$ = Legendre function of 1/2-integer order

$Q_m(r_1)$ = mth harmonic of blade cavity line source strength

r_1 = radius to propeller blade point in propeller coordinate system

r_o = radius to hull surface point in propeller coordinate system

r_{oj} = radius to jth hull contour segment in propeller system

r_h = propeller hub radius

r_t = propeller tip radius

R_e = denotes "real part" of complex number

$\vec{R}_1(t)$ = position vector to propeller blade point

$\vec{R}_o$ = position vector to hull surface point

$\vec{R}_{TE}$ = position vector to blade trailing edge

$\vec{R}$ = position vector to point in space

$S^*(\vec{R}_o)$ = surface of "double" hull

$\vec{S}_m$ = propeller blade operator used in formula reorganization

S_t = blade skew angle

s = subscript used in Legendre function expansions

t = time

TE = propeller blade trailing edge

T_n = nth blade rate harmonic of alternating thrust

$\vec{T}_m$ = vector representing mth propeller blade thickness harmonic

U = ship forward speed

U_o = mean tangential inflow velocity to propeller blade section

$\vec{v}_{i\nu}$ = νth harmonic of hull induced velocity field in propeller disk

$v_{i\nu x}, v_{i\nu r}, v_{i\nu \theta}$ = components of $\vec{v}_{i\nu}$ in propeller system

$\vec{v}_{jk}$ = 2-dimensional hull induced velocity on hull section

v_{jk}, w_{jk} = components of $\vec{v}_{jk}$ in hull coordinate system

v'_{jk}, w'_{jk} = components of $\vec{v}_{jk}$ in contour element coordinate system

$v^*_{30x}, v^*_{31\theta}$ = hull induced velocity harmonics at .7 propeller radius

$\vec{V}_{i\nu}$ = slipstream integral involving hull-induced velocity

x_1 = axial coordinate to propeller point in propeller system

x_o = axial coordinate to hull point in propeller system; also distance between propeller plane and waterline ending

x_{on} = axial coordinate to nth hull station

y_o = lateral distance between hull and propeller vertical centerplanes

y, z = hull contour coordinates

y', z' = hull contour coordinates in element system

z, z_{nj} = argument of Legendre function

z_o = vertical distance between water surface and propeller horizontal centerplane

α = propeller blade local cylindrical coordinate

α_ℓ = blade projected leading edge angle

α_t = blade projected trailing edge angle

α_o = cylindrical coordinate to hull surface point in hull system

$\vec{\alpha}_i$ = unit vector defining direction of excitation force

β = an integer

$\beta(r_1)$ = blade section geometric pitch angle

β_k = slope of kth hull contour segment

Γ = Gamma function

$\Delta_{\ell j}$ = length of jth hull section contour segment

ϵ_o = $\begin{matrix} 1/2 & \nu=0 \\ 1 & \nu>0 \end{matrix}$

η, ζ = dummy variables for y and z

η' = dummy variables for y' in hull contour element system

θ = angular position of propeller blade

θ_e = propeller position angle at which cavitation growth at r_1 commences

θ_c = propeller position angle at which cavitation collapse at r_1 commences

θ_t = propeller position angle at which cavitation collapse at r_1 is completed.

κ = propeller blade rake angle

μ = propeller blade dipole strength related to lift

μ_m = m^{th} harmonic of μ

ν = subscript denoting harmonic order

ξ = dummy variable for x_1

ρ = water density

ρ_o = radial coordinate to hull point in hull system

ρ_{jk} = distance between control point and source point on hull section contour

σ = propeller blade dipole strength related to thickness

σ_i = hull surface source density

σ_m = m^{th} harmonic if σ

$\vec{\tau}_p$ = unit vector tangent to propeller blade section pitch line

$\bar{\tau}$ = average cavity thickness at blade radius r_1

ϕ_i = hull induced potential field in propeller disk

$\phi_{i\nu}$ = ν^{th} harmonic of ϕ_i

ϕ_{30}^* = hull·induced potential harmonic at outer propeller radius

ω = angular velocity of propeller

HULL SURFACE FORCE FORMULA

In reference [1],[1] a method was proposed for calculating the unsteady propeller-induced forces acting on the surface of a ship stern. Formula (7) of that paper is:

$$F_{in} = \frac{N\omega}{\pi} \int_{-\pi/N\omega}^{\pi/N\omega} dt\ e^{-inN\omega t} \iint dS \left[\rho\sigma(\vec{R}_1)\frac{\partial}{\partial\tau_p} \right.$$
$$P(\vec{R}_1)$$
$$\left. + \frac{\mu(R_1)}{U}\int_{\xi=x_1}^{\infty} d\xi e^{inN\frac{\omega}{U}(x_1-\xi)}\frac{\partial}{\partial n_p} \right] H_{in}(\vec{R}_1) \qquad (1)$$

where F_{in} is the amplitude of the total unsteady hull surface force in direction i and at the nth harmonic of propeller blade rate frequency.

As explained in [1], the right-hand side of equation (1) involves an integration over the propeller blades and slipstream. All of the variables on the right-hand side, except the last one, H_{in}, are related to propeller blade geometry or loading. The hull is introduced in equation (1) through the function H_{in}. $H_{in}(\vec{R})$ is the amplitude of the unsteady fluid velocity potential resulting from the bare ship hull traveling backwards with speed U across the water surface and oscillating with unit amplitude in the direction i, and at the frequency harmonic n, of the excitation force of interest, F_{in}.

This formula is exact within the linear ideal fluid theory for given propeller characteristics. The hull and water surface boundary conditions will be satisfied through the H_{in} function by solving the hydrodynamics problem described in the previous paragraph.

Equation (1) is not completely general, however. The dipole representation of the propeller thickness effect, $\sigma(\vec{R}_1)$ in (1), does not allow completely for the existence of propeller blade cavitation, as explained in the Appendix.

Furthermore, the triple and quadruple integrals in (1) imply a somewhat laborious computation for a general ship hull if (1) is executed by purely numerical methods. As shown in the Appendix, the first integral in (1) can be performed analytically, thus reducing the computational effort.

The generalized and reorganized form of (1), which is developed in the Appendix, is the following:

---

[1]Numbers in brackets denote references at end of text.

I-3

$$F_{in} = \frac{N}{2} \int_{r_1=r_h}^{r_t} \left[\sum_{\nu=0}^{nN} \left(\vec{K}_{nN-\nu} \cdot \vec{v}_{i\nu} - \rho i n N \omega Q_{nN-\nu} \phi_{i\nu} e^{i\nu\alpha t} \right) \right.$$

$$+ \sum_{\nu=nN}^{\infty} \left(\vec{K}_{\nu-nN} \cdot \vec{v}_{i\nu} - \rho i n N \omega Q_{\nu-nN} \phi_{i\nu} e^{i\nu\alpha t} \right)$$

$$\left. + \sum_{\nu=0}^{\infty} \left(\vec{K}_{\nu+nN} \cdot \vec{v}_{i\nu} - \rho i n N \omega Q_{\nu+nN} \phi_{i\nu} e^{-i\nu\alpha t} \right) \right] dr_1 \tag{2}$$

F_{in} by (2) involves an integration over the radius of one propeller blade of sums of products of functions which pertain entirely to the propeller, $\vec{K}_m$ and Q_m, with functions which pertain entirely to the bare hull, $\vec{v}_{i\nu}$ and $\phi_{i\nu}$.

$\vec{v}_{i\nu}(r_1)$ and $\phi_{i\nu}(r_1)$ in (2) are the νth harmonics of the fluid velocity and fluid potential function, respectively, at radius r_1 in the propeller disk due to the bare hull moving with unit velocity in the direction, i, of the excitation force of interest. The Fourier series of which $\vec{v}_{i\nu}$ and $\phi_{i\nu}$ are components is in the angular coordinate in the propeller disk. $\vec{v}_{i\nu}$ and $\phi_{i\nu}$ can be computed for a given hull as described in the Appendix.

$Q_m(r_1)$ in (2) is the mth harmonic of the first time derivative of the blade cross-sectional area at radius r_1. The blade is considered as a "pseudo-blade" composed of the material blade plus any attached cavitation. Therefore, the blade cross-sectional area will be time dependent only where unsteady cavitation exists; Q_m in (2) will be zero for a non-cavitating propeller.

The $\vec{K}_m(r_1)$ in (2) is,

$$\vec{K}_m = \rho i n N \omega T_m \vec{\tau}_p + L_m \vec{n}_p \tag{3}$$

$\vec{\tau}_p(r_1)$ and $\vec{n}_p(r_1)$ in (3) are unit vectors at the propeller blade section at radius r_1. $\vec{\tau}_p$ is the unit tangent vector to the blade pitch line at r_1 and $\vec{n}_p$ is the unit normal vector to the blade pitch surface at radius r_1; refer to Figure 8 of the Appendix. The T_m and L_m in (3) are,

$$\begin{Bmatrix} T_{nN-\nu}(r_1) \\ L_{nN-\nu}(r_1) \end{Bmatrix} \equiv \frac{r_1}{\cos\beta} \int_{\alpha=\alpha_\ell}^{\alpha_t} \begin{Bmatrix} \sigma_{nN-\nu}(r_1,\alpha) \\ \mu_{nN-\nu}(r_1,\alpha) \end{Bmatrix} e^{i\nu\alpha} d\alpha$$

$$\begin{Bmatrix} T_{\nu-nN}(r_1) \\ L_{\nu-nN}(r_1) \end{Bmatrix} \equiv \frac{r_1}{\cos\beta} \int_{\alpha=\alpha_\ell}^{\alpha_t} \begin{Bmatrix} \bar{\sigma}_{\nu-nN}(r_1,\alpha) \\ \mu_{\nu-nN}(r_1,\alpha) \end{Bmatrix} e^{i\nu\alpha} d\alpha$$

$$\begin{Bmatrix} T_{\nu+nN}(r_1) \\ L_{\nu+nN}(r_1) \end{Bmatrix} \equiv \frac{r_1}{\cos\beta} \int_{\alpha=\alpha_\ell}^{\alpha_t} \begin{Bmatrix} \sigma_{\nu+nN}(r_1,\alpha) \\ \mu_{\nu+nN}(r_1,\alpha) \end{Bmatrix} e^{-i\nu\alpha} d\alpha \tag{4}$$

The T_m and L_m functions are integrals over the blade section at r_1 involving the mth harmonics of the strengths of the blade tangential and normal dipoles, σ and μ from (1) respectively. σ_m represents blade thickness effects and μ_m represents blade lift. The relationship between the σ_m in (4) and the Q_m in (2) is described in the Appendix.

AN EXACT ANALYTICAL EVALUATION

Equation (2) will require numerical evaluation for any case which is at all general. However, for the very simple case of a large flat plate above the propeller, an analytic evaluation of (2) is both easy and enlightening.

Consider the configuration shown on Figure 1. The propeller axis lies at a distance z_o beneath and parallel to a strip whose length is infinite and whose width is 2ℓ. The vertical force on the strip will be evaluated in the limit of large ℓ/z_o.

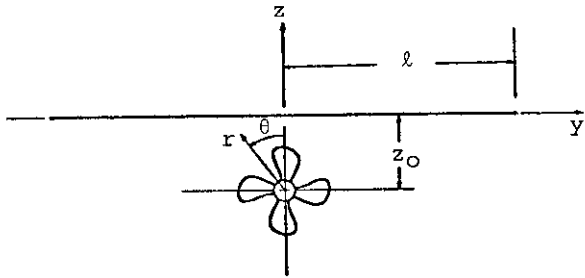Figure 1. Wide Flat Strip

The fluid velocity and potential function required in (2) for vertical force analysis (i=3) is that corresponding to vertical translation of the strip with unit downward velocity. The velocity potential, for z_o negative (Figure 1), is,

$$\phi_3 = R_e F(\zeta) \tag{5}$$

with

$$F(\zeta) = i(\zeta + \sqrt{\zeta^2 - \ell^2}) \tag{6}$$

and $\zeta = y + iz$

The velocity vector is,

$$\vec{v}_3 = \vec{\nabla}\phi_3 = v_{3y}\vec{j} + v_{3z}\vec{k}$$

with components,

$$v_{3y} = R_e F'(\zeta), \quad v_{3z} = -\text{Im}F'(\zeta) \tag{7}$$

where $F'(\zeta)$ is obtained from (6) by differentiation,

$$F'(\zeta) = i\left[1 + \frac{\zeta}{\sqrt{\zeta^2 - \ell^2}}\right] \tag{8}$$

The field points ζ in (6), (7), and (8) correspond to points in the propeller disk centered at $\zeta = -z_o i$. For $\ell \gg |\zeta|$, (6) and (8) become,

$$\lim_{\ell \to large} F(\zeta) = -\ell$$

$$\lim_{\ell \to large} F'(\zeta) = i$$

Therefore, in the limiting case of the infinite flat plate, for which $\ell \rightarrow \infty$, the fluid potential and velocities over the propeller disk are,

$$\phi_3 = -\ell \quad , \quad \vec{v}_3 = -\vec{k} \qquad (9)$$

In the propeller coordinate system, Figure 1,

$$\vec{k} = \cos\theta \ \vec{e}_r - \sin\theta \ \vec{e}_\theta \qquad (10)$$

$\vec{v}_{3\nu}$ and $\phi_{3\nu}$ are required in (2). By definition,

$$\vec{v}_{3\nu} = \frac{\varepsilon_0}{\pi} \int_{-\pi}^{\pi} \vec{v}_3 \ (\theta) e^{-i\nu\theta} d\theta \qquad (11)$$

with

$$\varepsilon_0 = \begin{cases} 1 & \nu > 0 \\ \frac{1}{2} & \nu = 0 \end{cases}$$

Combining (9), (10), and (11),

$$\vec{v}_{3\nu} = -\frac{\varepsilon_0}{\pi}\vec{e}_r \int_{-\pi}^{\pi} \cos\theta e^{-i\nu\theta}d\theta + \frac{\varepsilon_0}{\pi}\vec{e}_\theta \int_{-\pi}^{\pi} \sin\theta e^{-i\nu\theta}d\theta$$

Integrating,

$$\vec{v}_{3\nu} = \begin{cases} 0 & \nu \neq 1 \\ -(\vec{e}_r + i\vec{e}_\theta) & \nu = 1 \end{cases} \qquad (12)$$

Likewise, for $\phi_{3\nu}$

$$\phi_{3\nu} = \frac{\varepsilon_0}{\pi} \int_{-\pi}^{\pi} \phi_3(\theta) e^{-i\nu\theta} d\theta$$

Substituting (9),

$$\phi_{3\nu} = \begin{cases} 0 & \nu \neq 0 \\ -\ell & \nu = 0 \end{cases} \qquad (13)$$

Substitute (12) and (13) into (2),

$$F_{3n} = \frac{N}{2} \int_{r_1 = r_h}^{r_t} [(\vec{K}_{nN-1} \cdot \vec{v}_{31} - \rho i n N \omega Q_{nN} \ \phi_{30})$$
$$+ (\vec{K}_{1+nN} \cdot \vec{v}_{31} - \rho i n N \omega Q_{nN} \ \bar{\phi}_{30})] dr_1 \qquad (14)$$

The effects of blade cavitation are represented in (14) both in the source strength harmonics, Q_{nN}, and in the $\vec{\tau}_p$ component of the $\vec{K}_m$ vectors by (3) and (4). In fact, the T_m coefficients of $\vec{\tau}_p$ in (3) will involve only cavitation effects at $m = nN+1$ and $m = nN-1$, (14), since the thickness of the material blade is time independent and therefore contributes only to the $m=0$ term of T_m. Then, considering (12) and (13) and the fact that ℓ is large, the cavitation effects will be dominated by the source terms in (14). (14) can therefore be separated into cavitating (C) and non-cavitating (NC) components as,

$$F_{3n}^{NC} = \frac{N}{2} \int_{r_1 = r_h}^{r_t} (L_{nN-1}\vec{n}_p \cdot \vec{v}_{31} + L_{nN+1}\vec{n}_p \cdot \vec{v}_{31}) dr_1 \qquad (15)$$

and

$$F_{3n}^{C} = -\frac{i\rho n N^2 \omega}{2} \int_{r_1 = r_h}^{r_t} Q_{nN}(\phi_{30} + \bar{\phi}_{30}) dr_1 \qquad (16)$$

Considering first the cavitating component, (16),

$$\phi_{30} = \bar{\phi}_{30} = -\ell \qquad \text{by (13)}.$$

Therefore,

$$F_{3n}^{C} = i\rho n N^2 \omega \ell \int_{r_1 = r_h}^{r_t} Q_{nN}(r_1) dr_1 \qquad (17)$$

But as previously stated, and as shown in the Appendix, Q_m is just the mth harmonic of the 1st time derivative of the cavity cross-sectional area at r_1. The integral in (17) is therefore the mth blade-rate harmonic of the first time derivative of the total cavity volume on one blade,

$$\dot{V}_{nN} \equiv \int_{r_1 = r_h}^{r_t} \dot{A}_{nN}(r_1) dr_1 = \int_{r_1 = r_h}^{r_t} Q_{nN}(r_1) dr_1$$

(17) is therefore,

$$F_{3n}^{C} = i\rho n N^2 \omega \ell \dot{V}_{nN} \qquad (18)$$

(18) implies that the cavitation induced vertical force on the infinite strip, whose width, 2ℓ, is large compared to the propeller submergence, z_0 (Figure 1), is simply proportional to the width of the strip.

Consider now the non-cavitating force, (15). $\vec{n}_p$, from the Appendix, is,

$$\vec{n}_p = \frac{2\pi r_1 \vec{i} - P\vec{e}_\theta}{\sqrt{4\pi^2 r_1^2 + P^2}}$$

where P is the blade geometric pitch at r_1. Blade rake has been ignored in the above expression for $\vec{n}_p$.

Defining $\beta(r_1)$ as the geometric pitch angle at r_1, $\vec{n}_p$ can be written,

$$\vec{n}_p = \cos\beta \ \vec{i} - \sin\beta \ \vec{e}_\theta$$

Then, with $\vec{v}_{31}$ defined by (12), (15) becomes

$$F_{3n}^{NC} = \frac{iN}{2} \int_{r_1 = r_h}^{r_t} (L_{nN-1} - L_{nN+1}) \sin\beta \ dr_1$$

Inserting the L_m functions from (4),

$$F_{3n}^{NC} = \frac{iN}{2}\int_{r_1=r_h}^{r_t} r_1\tan\beta\int_{\alpha=\alpha_\ell}^{\alpha_t} \mu_{nN-1}e^{i\alpha}d\alpha dr_1$$

$$\hspace{4cm}(19)$$

$$-\frac{iN}{2}\int_{r_1=r_h}^{r_t} r_1\tan\beta\int_{\alpha=\alpha_\ell}^{\alpha_t} \mu_{nN+1}e^{-i\alpha}d\alpha dr_1$$

But (19) is just the negative of the nth blade rate harmonic of the vertical propeller bearing force due to propeller blade lift, [2]. The result, (19), is therefore in agreement with Breslin's condition, [3], that the net vertical force (bearing force plus surface force) corresponding to a propeller operating beneath an infinite flat plate is zero.

Equation (18) suggests on the other hand, however, that Breslin's condition does not hold for a cavitating propeller. By (18), the vertical cavity induced force on the infinite flat plate is itself infinite. But it is known that while very large surface forces are associated with moderate sheet cavitation, there is no corresponding large effect on propeller bearing forces. This seeming inconsistency was very adequately explained by the late Professor F.M. Lewis in a written discussion of reference [1]:

> By the Breslin condition it is evident that the total (net, non-cavitating) force will be the momentum force of the vertical motion of the free water surface outside the ship. If the wave patterns on the free surface produced by the propeller could be determined, the total force could be calculated from this.
>
> For cavitating conditions, either steady or intermittent, the problem becomes enormously more difficult. The Breslin condition does not hold because momentum forces are produced by motion of the surface of the cavities. I suspect that the vertical force will be greatly increased.

APPROXIMATE EVALUATION

Formulas (18) and (19) of the previous section, which apply to the vertical force on an infinitely long strip whose width is large compared to the propeller dimensions, are simple and convenient. However, even though the wide strip can be physically related to a wide ship stern in a limiting sense, (18) and (19) should not be expected to produce very realistic force estimates if applied to a typical ship.

An alternative is to compute (2) directly, using the procedures described in the Appendix. However, an approximate reduction of (2), similar to that performed for the strip in the previous section, yet not so extreme, is possible.

The velocity vector in (2), in the propeller coordinate system, is written,

$$\vec{v}_{i\nu} = v_{i\nu x}\vec{i} + v_{i\nu r}\vec{e}_r + v_{i\nu\theta}\vec{e}_\theta$$

with

$$v_{i\nu\theta} = \frac{i\nu}{r_1}\phi_{i\nu}$$

For the flat plate, the Fourier series in ν, of which $\vec{v}_{i\nu}$ and $\phi_{i\nu}$ are components, are composed of single terms, as shown by (12) and (13). For a general ship stern, instead of a flat plate, $\vec{v}_{i\nu}$ and $\phi_{i\nu}$ will, in general, be non-zero for all ν. However, for a ship stern which is "flat-plate like," the Fourier series on $\vec{v}_{i\nu}$ and $\phi_{i\nu}$ will converge rapidly from the leading terms. For the vertical case, i=3, the leading terms in the series are $\nu=0$ for $v_{3\nu x}$, $v_{3\nu r}$, and $\phi_{3\nu}$, and $\nu=1$ for $v_{3\nu\theta}$, since $v_{i0\theta}\equiv 0$. For a ship whose stern is characterized as broad and flat, these leading terms will be the dominant terms. If only these leading terms are carried in (2), (2) reduces to,

$$F_{3n} = \frac{N}{2}\int_{r_1=r_h}^{r_t} (\vec{K}_{nN}\cdot v_{30x}\,\vec{i} + K_{nN-1}\cdot v_{31\theta}\vec{e}_\theta$$

$$\hspace{4cm}(20)$$

$$-\rho inN\omega Q_{nN}\phi_{30} + \vec{K}_{nN}\cdot\bar{v}_{30x}\,\vec{i}$$

$$+\vec{K}_{1+nN}\cdot\bar{v}_{31\theta}\vec{e}_\theta - \rho inN\omega Q_{nN}\bar{\phi}_{30})dr_1$$

The radial velocity component has not been carried in (20) since the $\vec{K}_m$ vectors do not contain a radial component.

As in the case of the flat plate, the dipole terms in the $\vec{K}_m$ in (20) pertaining to blade thickness are associated entirely with unsteady cavitation at m=nN-1, nN, and nN+1. The force due to cavitation should, as in the case of the plate, be dominated by the source term, Q_m in (20), when the ship stern is broad and flat. Therefore, representing the cavitation effects entirely by the source terms, the vertical force separates into cavitation and non-cavitation parts as,

$$F_{3n}^{NC} = N\int_{r_1=r_h}^{r_t} L_{nN}\,v_{30x}(\vec{n}_p\cdot\vec{i})dr_1$$

$$+\frac{N}{2}\int_{r_1=r_h}^{r_t} L_{nN-1}v_{31\theta}(\vec{n}_p\cdot\vec{e}_\theta)dr_1 \hspace{1cm}(21)$$

$$+\frac{N}{2}\int_{r_1=r_h}^{r_t} L_{nN+1}\bar{v}_{31\theta}(\vec{n}_p\cdot\vec{e}_\theta)dr_1$$

and

$$F_{3n}^{C} = -\rho i n N^2 \omega \int_{r_1=r_h}^{r_t} Q_{nN}\, \phi_{30}\, dr_1 \qquad (22)$$

Advantage has been taken of the fact in (21) and (22) that both v_{30x} and ϕ_{30} are pure real so that

$$\bar{v}_{30x} = v_{30x}$$

and

$$\bar{\phi}_{30} = \phi_{30}$$

It has been observed that the potential and velocity components in (21) and (22) do not vary greatly over the propeller radius. Therefore, replace these functions by some average radial values: v_{30x}^{*}, $v_{31\theta}^{*}$, and ϕ_{30}^{*} . Typically,

$$v_{30x}^{*} = v_{30x}(r_1)\Big|_{r_1 \approx .7r_t}$$

$$v_{31\theta}^{*} = v_{31\theta}(r_1)\Big|_{r_1 \approx .7r_t}$$

$$\phi_{30}^{*} = \phi_{30}(r_1)\Big|_{r_1 > .7r_t}$$

The suggestion that the potential be evaluated at a larger radius than the velocities is because cavitation, with which ϕ_{30} is associated, is typically distributed more toward the blade tip. However, since these functions usually vary slowly with radius, the selection criterion should not be critical.
(21) and (22) then become, with $\vec{n}_p = \cos\beta\,\vec{i} - \sin\beta\,\vec{e}_\theta$,

$$F_{3n}^{NC} = \left[N\int_{r_1=r_h}^{r_t} L_{nN}\,\cos\beta\, dr_1 \right] v_{30x}^{*}$$

$$- \left[\frac{N}{2}\int_{r_1=r_h}^{r_t} L_{nN-1}\,\sin\beta\, dr_1 \right] v_{31\theta}^{*} \qquad (23)$$

$$- \left[\frac{N}{2}\int_{r_1=r_h}^{r_t} L_{nN+1}\,\sin\beta\, dr_1 \right] \bar{v}_{31\theta}^{*}$$

and

$$F_{3n}^{C} = \left[-\rho i n N^2 \omega \int_{r_1=r_h}^{r_t} Q_{nN}\, dr_1 \right] \phi_{30}^{*}$$

or

$$F_{3n}^{C} = -\rho n N^2 \omega\, \dot{\vec{V}}_{nN}\, \phi_{30}^{*} \qquad (24)$$

F_{3n}^{C} by (24) bears a strong resemblance to (18), which was developed for the wide strip of width 2ℓ. (24) reduces to (18) if ϕ_{30}^{*} is replaced by $-\ell$. The definition of ℓ can be generalized to apply to a ship as, say, the offset to the design waterline at a station corresponding to the vertical plane of the propeller disk. With this definition, $|\phi_{30}|$ should always be less than ℓ.

Formula (24) is equivalent to the result obtained by Breslin in [4] when specialized to a flat plate of infinite length, but whose width, compared to the propeller dimensions, is not necessarily large. In that case, referring to Figure 1,

$$\phi_{30}^{*} = -(\sqrt{z_0^{\,2}+\ell^2} - z_0)$$

which can be obtained from (5) and (6) by setting $\zeta = -iz_0$. This is the same as Breslin's potential A_0 in [4], excluding an erroneous factor of 2. An improvement over (18) for a flat plate of finite width should therefore be,

$$F_{3n}^{C} = \rho i n N^2 \omega\, \dot{\vec{V}}_{nN}\,(\sqrt{z_0^{\,2}+\ell^2} - z_0) \qquad (18a)$$

Turning to the non-cavitating force, (23), and substituting the L_m from (4),

$$F_{3n}^{NC} = \left[N\int_{r_1=r_h}^{r_t}\int_{\alpha=\alpha_\ell}^{\alpha_t} \mu_{nN}\,d\alpha\, dr_1 \right] v_{30x}^{*}$$

$$+ \left[-\frac{N}{2}\int_{r_1=r_h}^{r_t}\tan\beta\int_{\alpha=\alpha_\ell}^{\alpha_t} \mu_{nN-1}\,e^{i\alpha}\,d\alpha\, dr_1 \right] v_{31\theta}^{*}$$

$$\qquad\qquad (25)$$

$$+ \left[-\frac{N}{2}\int_{r_1=r_h}^{r_t} r_1\tan\beta\int_{\alpha=\alpha_\ell}^{\alpha_t} \mu_{nN+1}\,e^{-i\alpha}\,d\alpha\, dr_1 \right] \bar{v}_{31\theta}^{*}$$

The second and third bracketed terms in (25) can be related to the vertical propeller bearing force by comparison with (19). The vertical flat plate force, (19), has been identified as the negative of the propeller vertical bearing force. Denoting the amplitude of the nth blade rate harmonic of the propeller vertical bearing force as, F_{vbn},

$$F_{vbn} = F_{vbn}^{-} + F_{vbn}^{+}$$

where the two terms are the contributions of the $nN-1$ and $nN+1$ blade pressure, or wake, harmonics, respectively.

$$F_{vbn}^- = -\frac{iN}{2} \int_{r_1=r_h}^{r_t} r_1 \tan\beta \int_{\alpha=\alpha_\ell}^{\alpha_t} \mu_{nN-1} e^{i\alpha} d\alpha dr_1$$

$$(26)$$

$$F_{vbn}^+ = \frac{iN}{2} \int_{r_1=r_h}^{r_t} r_1 \tan\beta \int_{\alpha=\alpha_\ell}^{\alpha_t} \mu_{nN+1} e^{-i\alpha} d\alpha dr_1$$

Recognizing additionally that the first bracketed term in (25) is just the negative of the amplitude of the nth blade-rate harmonic of the alternating thrust, T_n,

$$T_n = -N \int_{r_1=r_h}^{r_t} r_1 \int_{\alpha=\alpha_\ell}^{\alpha_t} \mu_{nN} d\alpha dr_1$$

(25) can be written,

$$F_{3n}^{NC} = -T_n v_{30x}^* - iF_{vbn}^- v_{31\theta}^* + iF_{vbn}^+ v_{31\theta}^*$$

$$(27)$$

If the alternating thrust and vertical bearing force for a propeller operating in a specified ship wake have been estimated, then (27) provides a means of estimating the corresponding non-cavitating vertical hull surface force, if the velocity harmonics in (27) corresponding to the particular bare-hull can be estimated.

Note that (27) degenerates to (19) in the case of an infinite flat plate. For the infinite flat plate $v_{30x}^*=0$ and $v_{31\theta}^*=-i$, by (12).

EVALUATION OF APPROXIMATE METHODS
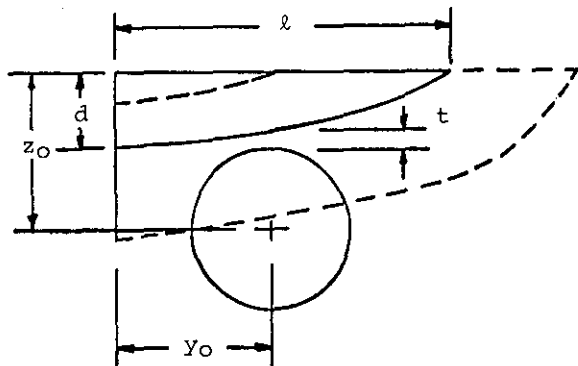
The formula (2) has been applied to a number of ships over the past several years. The calculated data corresponding to four of these applications is used to compare the approximate formulas for the vertical hull surface force, (24) and (27), and also (18), (18a), and (19), with the more accurate evaluations by (2) directly.

The four ships chosen are two with twin propellers and two with single propellers. The twin-screw ships are a large coastal ferry and a naval cruiser. The single-screw ships are a Great Lakes ore-carrier and a containership. The pertinent geometric characteristics of the four ships, including the hull velocity and potential data required in (24) and (27), is given on Figures 2, 3, 4, and 5. Note that the sterns of three of the ships would be characterized as flat-plate-like, while one, that of the containership, would not. The pertinent propeller data for each of the four ships is given in Tables I, III, VI, and VIII. The calculated vertical surface forces for each case are compared in Tables II, IV, V, VII and IX; the force amplitudes are expressed as percentages of steady thrust as indicated on the tables.

Each of the four cases are described individually as follows:

Ship I - Twin-Screw Ferry (Figure 2)

The blade rate harmonic, n=1, of the bearing forces and vertical non-

GEOMETRIC DATA

x_o/ℓ	1.047	D/ℓ [1]	.450
y_o/ℓ	.457	t/D	.127
z_o/ℓ	.457		
d/ℓ	.219		
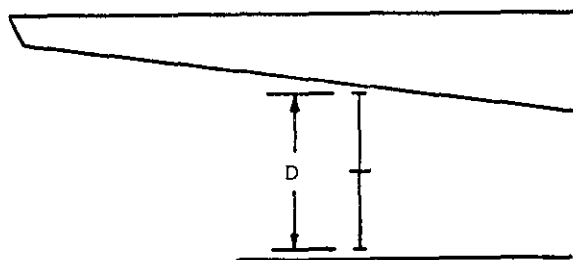
HULL POTENTIAL AND VELOCITY DATA
(VERTICAL FORCE ANALYSIS)

v_{30x}^*	.316
$v_{31\theta}^*$	-.423 -.586i
$\phi_{30/\ell}^*$	-.604

[1] D CORRESPONDING TO PROP 1, TABLE I

Figure 2. Coastal Ferry

cavitating surface force was calculated for three different 5-bladed propellers. The characteristics of the three propellers are given in Table I. The three propellers, identified as 1, 2, and 3, are all about the same diameter, with propeller 1 being slightly larger than 2 and 3, which are the same diameter. Propeller 1 is essentially unskewed and delivers a lower power at a lower RPM than propellers 2 and 3. Propeller 2 has moderate skew and propeller 3 is unskewed.

	PROP 1	PROP 2	PROP 3[1]
NO OF BLADES, N	5	5	5
DIAMETER, D (m)	2.64	2.53	2.53
	(8.23 ft)	(7.87 ft)	(7.87 ft)
% SKEW[2]	20.2	55.9	0
RPM	275	320	320
SHP	3330	4080	4080

1. PROP 3 IDENTICAL TO PROP 2 WITH SKEW = 0
2. % SKEW = (ST·N/360) × 100
   St = SKEW ANGLE OF BLADE TIP IN PROJECTED PLANE (DEG)

TABLE I
Ship I - Twin-Screw Coastal Ferry
Propeller Data

Table II compares the blade rate (n=1) vertical surface forces calculated by (2) versus the more approximate predictions by (27) and the flat plate formula (19).

Ship II - Single-Screw Great Lakes Ore Carrier (Figure 3)

This ship is the subject of reference [5]. The ship experienced bad cavitation induced stern vibration on the builder's sea trails. An abbreviated stern tunnel was added above the propeller (Figure 3) to improve the wake in the propeller disk, and thereby reduce the severity of the cavitation and resultant vibration.

Force calculations were performed for the "without" and "with" tunnel configurations. Bearing forces and the vertical component of the hull surface force were calculated for both stern configurations. Both blade-rate and twice-blade rate harmonics were calculated, and the effects of cavitation were included in the hull surface force calculations.

Figure 3 shows the geometric characteristics of the ship stern. Two sets of hull velocity and potential data, for use in (24) and (27), are listed on Figure 3; these correspond to the "without" and "with" tunnel configurations, as indicated.

Table III lists the pertinent propeller characteristics.

NO OF BLADES, N	4[1]
DIAMETER, D (m)	6.42 (20 ft)
Ae/Ao	.581
% SKEW	4.3
RPM	120
SHP	14,000

1. CONTROLLABLE PITCH, LEFT-HAND ROTATION

TABLE III
Ship II - Single-Screw Great Lakes Ore
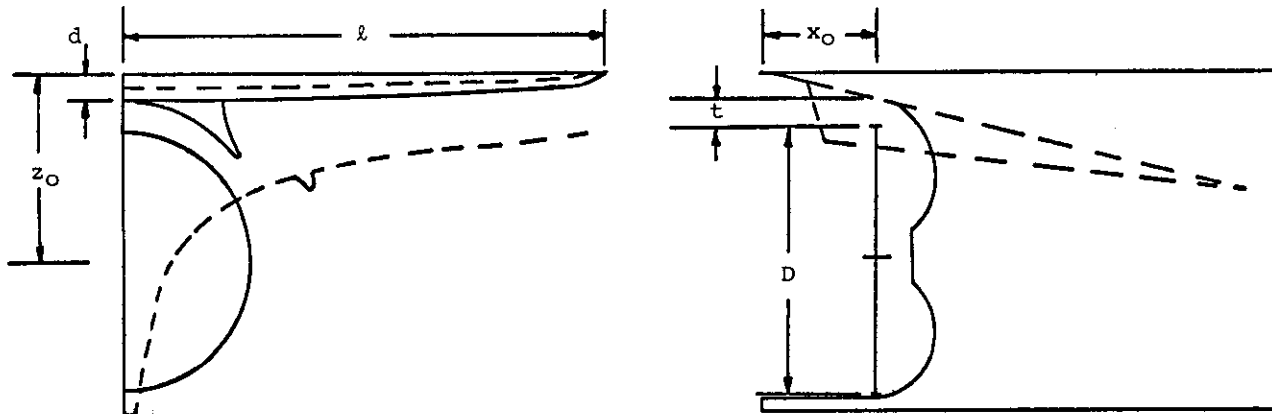Carrier
Propeller Data

Tables IV and V show the comparisons of the vertical surface forces calculated by (2), from [5], and by the approximate formulas (18), (18a), (19), (24), and (27). The non-cavitating forces are shown in Table IV and the corresponding forces due to cavitation are shown in Table V.

It can be noted in Table IV that the same bearing force components are listed for both the without and with

	PROP 1				PROP 2				PROP 3			
	RE	IM	AMP	PHASE	RE	IM	AMP	PHASE	RE	IM	AMP	PHASE
BEARING FORCE COMPONENTS												
F_{vb1}^{-}	-.23	-1.1			.15	-.11			-1.9	.03		
F_{vb1}^{+}	.11	.16			-.21	.03			.11	-.11		
T_1	-1.1	-.41			.11	-.99			-.30	1.2		
F_{31} bY (2)[2]	1.2	1.3	1.8	-9.6	-.34	.65	.73	-23.	1.9	-1.3	2.3	6.7
F_{31} bY (27) $\overline{-T_1 v_{30x}^* - iF_{vb1}^- v_{316}^*}$ $+iF_{vb1}^+ v_{316}^*$	.96	.56	1.1	-6.1	.06	.51	.52	-17.	1.1	-1.2	1.6	9.5
F_{31} bY (19) $\overline{-F_{vb1}^- - F_{vb1}^+}$	.12	.98	.99	-17.	.063	.079	.10	-10.	1.8	.080	1.8	-.51

1. $f_{3n}(t)$ = AMP·COS nN (ωt-PHASE); AMP PERCENT OF STEADY THRUST; PHASE = 57.3·[TAN^{-1}(-IM/RE)]/nN (DEGREES) = POSITION OF BLADE NEAREST TOP-DEAD-CENTER WHEN f(t) IS POSITIVE MAXIMUM.
2. 16 Lm HARMONICS (m=0 TO 15) AND 1 Tm HARMONIC (m=0) USED IN (2).

TABLE II Ship I - Twin-Screw Coastal Ferry
Non-Cavitating Blade-Rate Vertical Surface Forces[1]
(Refer to Figure 1 and Table I)

GEOMETRIC DATA

x_O/ℓ	.237	D/ℓ	.526
z_O/ℓ	.375	t/D	.113
d/ℓ	.053		

HULL POTENTIAL AND VELOCITY DATA
(VERTICAL FORCE ANALYSIS)

	W/O TUNNEL	WITH TUNNEL
v_{30x}^{*}	.752	.690
$v_{31\theta}^{*}$	-.585i	-.491i
$\phi_{30/\ell}^{*}$	-.633	-.590

Figure 3.   Great Lakes Ore Carrier

	BLADE-RATE (n=1)								TWICE-BLADE-RATE (n=2)							
	W/O TUNNEL				WITH TUNNEL				W/O TUNNEL				WITH TUNNEL			
	RE	IM	AMP	PHASE[2]	RE	IM	AMP	PHASE	RE	IM	AMP	PHASE	RE	IM	AMP	PHASE
BEARING FORCE COMPONENTS																
F_{vbn}^-	1.4	.56			1.4	.56			-.005	-.44			-.005	-.44		
F_{vbn}^+	-1.6	-.29			-1.6	-.29			.16	.14			.16	.14		
T_n	-2.5	2.1			-2.5	2.1			1.4	-.086			1.4	-.086		
F_{3n} bY (2)[1]	1.4	.59	1.5	5.6	.14	.072	.16	6.8	-1.1	.33	1.1	20.	-1.0	.17	1.0	21.
F_{3n} bY (27)	2.1	-1.7	2.7	-10.	1.9	1.6	2.4	10.	-1.1	.24	1.2	21.	-1.0	.21	1.1	21.
$-T_n v_{30x}^* + iF_{vbn}^- v_{31\theta}^* + iF_{vbn}^+ \bar{v}_{31\theta}^*$																
F_{3n} bY (19) $-F_{vbn}^- - F_{vbn}^+$	.25	-.26	.36	-12.	.25	-.26	.36	-12.	-.15	.31	.34	15.	-.15	.31	.34	15.

1. FORCES PERCENT OF STEADY THRUST
2. PHASE = $-57.3 \cdot \text{TAN}^{-1}(-\text{IM}/\text{RE})/nN$ FOR LEFT-HAND ROTATION (SEE TABLE II)
3. 16 Lm HARMONICS (m=0 TO L5) AND 1 Tm HARMONIC (m=0) USED IN (2).

TABLE IV   Ship II – Single-Screw Great Lakes Ore Carrier
Non-Cavitating Vertical Surface Forces
(Refer to Figure 2 and Table III)

tunnel cases. The only model wake survey conducted was prior to the addition of the stern tunnel. The bearing forces were calculated from this wake survey and used for both stern configurations. The difference in surface forces shown on Table IV is therefore due entirely to the differences in diffraction effects of the two stern configurations.

In the cavitation force comparisons of Table V the volume variation $\ddot{\Psi}_{n4}$, as well as the Q_m and σ_m used in (2), were calculated by formulas proposed in reference [5]. Specifically,

$$\sigma_m(r_1,\alpha) = -\frac{2U_O\tau EXT}{m^2\pi}\left\{ e^{-im\theta_e}\left[\frac{1-e^{im(\theta_e-\theta_t)\sqrt{\frac{\alpha-\alpha\ell}{EXT}}}}{(\theta_e-\theta_t)^2}\right] - e^{-im\theta_c}\left[\frac{1-e^{im(\theta_c-\theta_t)\sqrt{\frac{\alpha-\alpha\ell}{EXT}}}}{(\theta_c-\theta_t)^2}\right]\right\}$$

I-10

	BLADE RATE (n=1)								TWICE-BLADE-RATE (n=2)							
	W/O TUNNEL				WITH TUNNEL				W/O TUNNEL				WITH TUNNEL			
	RE	IM	AMP	PHASE	RE	IM	AMP	PHASE	RE	IM	AMP	PHASE	RE	IM	AMP	PHASE
F_{3n} bY (2)[1]	-1.5	21.	21.	24.	-8.	1.6	8.1	42.	-4.9	11.	12.	14.	.67	-.70	.97	-5.8
CAVITY VOLUME VARIATION $\dot{V}_{n4}$ (in³/sec)	6500.	440.			490.	1200.			1800.	860.			-110.	-150.		
$\dfrac{F_{3n} \text{ bY } (24)}{-\rho i n N^2 \omega \dot{V}_{n4} \phi_{30}^*}$	-1.1	16.	16.	24.	-7.1	1.1	7.2	43.	-4.3	9.0	10.	14.	.68	-.52	.86	-4.7
$\dfrac{F_{3n} \text{ bY } (18)}{\rho i n N^2 \omega \dot{V}_{n4} \ell}$	-1.7	26.	26.	24.	-12.	1.9	12.	43.	-6.8	14.	16.	14.	1.1	-.88	1.4	-4.7
$\dfrac{F_{3n} \text{ bY } (18a)}{\rho i n N^2 \omega \dot{V}_{n4}(\sqrt{\ell^2+Z_0^2}-Z_0)}$	-1.3	19.	19.	24.	-9.1	1.5	9.3	43.	-5.1	11.	12.	14.	.87	-.67	1.1	-4.7

1 FORCES PERCENT OF STEADY THRUST
2 PHASE = -57.3· TAN⁻¹(-IM/RE) /nN FOR LEFT HAND ROTATION (SEE TABLE II)
3 16 T_m AND Q_m HARMONICS (M=0 TO 15) USED IN (2).

TABLE V Ship II – Single·Screw Great Lakes Ore Carrier
Vertical Surface Forces Due to Cavitation
(Refer to Figure 2 and Table III)

$$Q_m(r_1) = \sigma_m(r_1, \alpha_t)$$

and

$$\dot{V}_{nN} = \int_{r_1=r_h}^{r_t} Q_{nN}(r_1) dr_1$$

where, as a function of radius,

$U_o(r_1)$ = mean inflow velocity tangent to pitch line at r_1

$\bar{\tau}(r_1)$ = average cavity thickness

$EXT(r_1) \equiv \alpha_t - \alpha_\ell$ = maximum angular extent, in the projected plane, of the cavity along the blade section

$\theta_e(r_1)$ = propeller position angle at which cavity growth begins

$\theta_c(r_1)$ = propeller position angle at which cavity collapse begins

$\theta_t(r_1)$ = propeller position angle at which cavity collapse is completed

This data for the ore carrier was estimated largely from photographs of model propeller cavitation tests as explained in [5]. Separate cavitation tests were performed with the two stern configurations (with and without tunnel), providing separate sets of cavitation data for the two cases.

Ship III – Twin-Screw Naval Cruiser
(Figure 4)
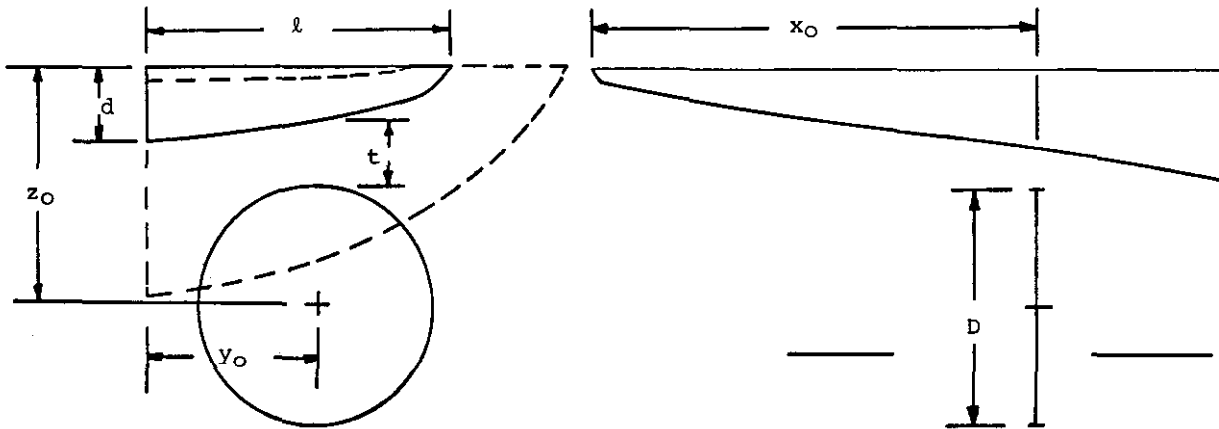
GEOMETRIC DATA

x_o/ℓ	1.483	D/ℓ	.756
y_o/ℓ	.567	t/D	.292
z_o/ℓ	.769		
d/ℓ	.252		

HULL POTENTIAL AND VELOCITY DATA
(VERTICAL FORCE ANALYSIS)

v_{30x}^* .146

$v_{31\theta}^*$ -.325 - .350i

ϕ_{30}^* -.518

Figure 4. Naval Cruiser

The blade-rate harmonic, n=1, of the bearing forces and vertical non-cavitating surface force was calculated for two different propellers. The characteristics of the two propellers are given on Table VI. The two propellers are of the same diameter, RPM, and power, but one is a 5-bladed propeller with high skew, and the other has 7-blades and zero skew.

	PROP 1	PROP 2
NO OF BLADES, N	5	7
DIAMETER, D (m)	5.78 (18ft)	5.78 (18ft)
% SKEW	76	0

[1]. RPM AND POWER SAME FOR BOTH PROPELLERS

TABLE VI
Ship III – Twin Screw Naval Cruiser Propeller Data[1]

Table VII compares the blade-rate vertical surface forces calculated by (2) versus the approximate formulas for both propellers.

Ship IV – Single-Screw Containership (Figure 5)

Figure 5 and Table VIII define the stern/propeller configuration for ship IV. The blade-rate and twice-blade-rate non-cavitating vertical hull surface forces calculated by the three methods, (2), (19), and (27), are com-

BEARING FORCE COMPONENTS	PROP 1				PROP 2			
	RE	IM	AMP	PHASE	RE	IM	AMP	PHASE
F_{vb1}^-	-.55	.18			.069	.11		
F_{vb1}^+	-.20	.24			.40	-.27		
T_1	-.54	.30			.82	.66		
F_{31} by (2)[2]	.15	-.24	.28	12.	-.40	-.20	.45	22.
F_{31} by (27) $-T_1 V_{30x} - iF_{vb1}^- V_{31\theta} + iF_{vb1}^+ V_{31\theta}$	.36	-.31	.48	8.0	-.42	-.14	.44	23.
F_{31} by (19) $-F_{vb1}^- - F_{vb1}^+$	.75	-.42	.86	5.9	-.49	.16	.52	-23.

1. FORCES PERCENT OF STEADY THRUST
2. 9 Lm HARMONICS (m=0 TO 8) AND 1 Tm HARMONIC (m=0) USED IN (2).

TABLE VII
Ship III - Twin-Screw Naval Cruiser Non-Cavitating Blade Rate Vertical Surface Forces
(Refer to Figure 4 and Table VI)

NO OF BLADES, N	6
DIAMETER, D (m)	7.55 (23.5 ft)
Ae/Ao	.744
% SKEW	39
RPM	108
SHP	27,800

TABLE VIII
Ship IV - Single-Screw Containership Propeller Data

GEOMETRIC DATA

x_o/ℓ	2.707	D/ℓ	3.00
z_o/ℓ	2.556	t/D	.096
d/ℓ	.767		

HULL POTENTIAL AND VELOCITY DATA
(VERTICAL FORCE ANALYSIS)

V_{30x}^* .153

$V_{31\theta}^*$ -.0192i

$\phi_{30/\ell}^*$ -.475

Figure 5. Containership

BEARING FORCE COMPONENTS	BLADE-RATE				2x BLADE-RATE			
	RE	IM	AMP	PHASE	RE	IM	AMP	PHASE
F_{vbn}	1.6	.97			.077	.069		
F_{vbn}^+	-.67	-.46			-.062	-.051		
τ_n	-4.9	-2.3			-.18	-.046		
F_{3n} by (2)[2]	-.40	2.7	3.0	-16.	-.16	.046	.16	-14.
F_{3n} by (27)	.73	.14	.01	-4.2	.027	.007	.028	-1.3
$-\tau_n \bar{v}_{3ux} - i F_{vbn} \bar{v}_{310}$ $+ i F_{vbn}^+ \bar{v}_{310}$								
F_{3n} by (19) $-F_{vbn} - F_{vbn}^+$	-.91	-.50	1.0	2.0	-.015	-.018	.027	11.

1. FORCES PERCENT OF STEADY THRUST

2. 16 Um HARMONICS (m=0 TO 15) AND 1 τ_n HARMONIC (m=0) USED IN (2).

TABLE IX
Ship IV - Single-Screw Containership
Non-Cavitating Vertical Surface Forces
(Refer to Figure 5 and Table VIII)

In the comparison of the vertical hull surface forces on Tables II, IV, V, VII, and IX, the predictions by (2) should be taken as the standard. No fewer than 9 terms on $\vec{K}_m$ and Q_m in (2) were used; the precise number in each case is indicated by footnotes on the respective tables. The essential step in reducing (2) to (24) and (27) was truncating the series in (2) at its leading terms in the hull-induced velocity and potential functions, (20). The differences between (2) and (24) and (27) are primarily a reflection of this truncation. The same propeller blade pressure distributions, μ_m, were used in (2) and (27); nine-point Simpson's rule integration was used both radially and chordwise in (2) and (4), as well as in the bearing force components of (19) and (27), which are given by (26). Likewise the same cavitation data and cavity model, from [5], were used in σ_m and Q_m of (2) and in $\vec{V}_{nN}$ of (18), (18a), and (24). The hull-induced velocity and potential data was the same for (2) versus (24) and (27), but with average radial values used in the truncated series of the approximate formulas (Figures 2 through 5). The hull-flow data was calculated for all cases by the procedures described in the Appendix.

DISCUSSION OF COMPARISONS

Non-Cavitating Forces

First of all, there is no consistent agreement at all between (2) and the flat-plate formula (19), either in an absolute or relative sense. Indeed, none should be expected. (19) is the negative of the vertical bearing force. Consistent agreement between (19) and (2) would therefore imply zero net vertical vibratory force on ships. This is, of course, not the case, in general. (19) is of value in the comparisons in establishing a lower bound on the capability of the theoretically more accurate approximation (27); the upper bound is established by (2).

Considering (27) versus (2), the agreement ranges from very poor on the single-screw containership to very good on the naval cruiser with the 7-bladed propeller. The performance of (27) should be expected to be poorest on the conventional stern ship. The "narrowness" of the counter of the containership stern violates the "broadness" assumption required in the reduction of (2) to (27). As previously stated, the Fourier series on the hull-induced flow field converges more rapidly when the stern is broad, relative to the propeller disk, versus narrow. The series truncation error in (27) is therefore less for the broader stern, and (27) should be more accurate for ships, I, II, and III, than for ship IV. This generality with regard to stern shape is contradicted by the case of the ore-carrier at blade-rate frequency; the barge stern of this ship would certainly be characterized as broad and flat. The primary reason for the poor agreement of (2) and (27) shown on Table IV is due to an unusually large blade thickness contribution, particularly in the "with tunnel" case, which is excluded by the truncation associated with (27). Note that the comparison at twice blade-rate frequency for the ore carrier shown on Table IV is quite good.

Cavitating Forces

While the comparisons are limited (Table V), the approximate evaluations of the vertical surface forces due to cavitation by (18a) and (24), both compare favorably to the more accurate evaluations by (2). The comparisons on Table V are probably indicative of the capability of the approximate formulas when applied to ships with broad flat sterns like that of the ore-carrier. Both (18a) and (24), and particularly the flat-plate formula (18a), would be expected to be considerably poorer if applied to a more conventional stern such as that of the containership, Figure 5.

For a conventional stern the zeroth harmonic potential in the propeller disk may not be the dominant flow harmonic that it is in the case of the broad flat open stern; compare the velocity and potential data tabulated on Figure 5 versus Figure 3. It is the dominance of ϕ_{30}^* over other harmonics of either the potential or velocity components in the case of the barge stern which produces the good agreement between (24) and (2) shown on Table V. Specifically, the dipole terms in (2), by way of the hull-induced velocity field, should play a much more important role in the cavitating hull-surface force on conventional stern ships.

Hull-Induced Flow Data

The hull induced velocity and potential data of Figures 2 through 5 is interesting in itself. It provides insight into the influence of certain characteristics of stern configuration on the vertical hull surface forces, at least for the broad flat stern type of Figures 2, 3, and 4. This is through the approximate formulas (24) and (27), which have been shown to be reasonably accurate, at least in a relative sense, for the broad flat stern type.

For the non-cavitating force, for example, (27) shows that the alternating thrust multiplies the zeroth harmonic of the axial hull-induced velocity in the disk, and sums with products of the vertical bearing force components and the first harmonic of the tangential hull flow velocity in the disk. For an infinite flat plate the tangential velocity approaches a limiting maximum absolute value of 1, (12). Therefore the magnitude of the tangential velocity, $v_{31\theta}^*$, for a particular hull, is indicative of the magnitude of a component of the vertical surface force relative to the vertical bearing force. That is, for a given vertical bearing force, the smaller $v_{31\theta}^*$, the smaller should be the bearing force related component of the surface force. In general, the narrower the waterplane aft, the smaller should be $v_{31\theta}^*$; this is confirmed by the data on Figures 2 through 5.

The axial velocity induced by an infinite flat plate or by any cylindrical body of infinite length is zero, and the alternating thrust does not contribute to the vertical surface force for such cases, by (27). If however, the body surface is terminated aft of the propeller disk, typically like the waterplane ending of a broad flat stern, an axial velocity will be induced which increases as the waterplane end is approached. This increasing axial velocity with decreasing inset, x_O/ℓ, is clearly shown on Figures 2, 3, and 4. Therefore, for a given alternating thrust, the closer is the propeller to the waterplane ending, the larger is the axial induced velocity, and the larger is the thrust contribution to the vertical surface force. [6]. Of course cancellation between the three components of (27) can occur, and usually does to some degree. Nevertheless, some useful rules of thumb are believed to be provided by the formula (27).

With regard to the cavitating hull-surface force, the zeroth harmonic of the hull induced potential in the propeller disk, ϕ_{30}, is the dominant hull effect, according to (24), for the broad flat stern. The potential approaches the negative of the waterplane half breadth as an upper limit, (13), and decreases with decreasing waterplane breadth, Figures 2, 3, and 4. The potential will also decrease on approach-ing the waterplane ending aft, but the decrease should typically be rather abrupt. The zeroth harmonic of the potential should be somewhat insensitive to the location of the disk relative to the waterplane ending for typical stern configurations. This is supported by the data on Figures 2, 3, and 4. Therefore, in converse to the non-cavitating force, the force due to cavitation, for given propeller cavitation characteristics, will be reduced on reducing the distance between the waterplane ending and the propeller disk, x_O/ℓ on the Figures. However, the controlling characteristic in the cavitating force should be the breadth of the waterplane aft.

CONCLUSION

The approximate formulas developed for calculating propeller-induced vertical hull-surface forces are reasonably valid, at least in a relative sense, for sterns which are broad and flat aft, typical of open strut or transom stern ships. The formulas are not valid for ships whose counter is narrow relative to the propeller diameter.

The hull-flow data required in the approximate formulas is in itself useful in qualitatively evaluating the relative merit of sterns with different but similar characteristics, independent of any particular propeller design.

The hull-flow data presented for the particular ships studied in this paper should be useful to the reader interested in approximating the hull-surface forces on similar sterns, for which propeller-bearing forces and/or propeller cavitation data is available.

ACKNOWLEDGEMENTS

REFERENCES

1. W.S. Vorus, "A Method for Analyzing the Propeller Induced Vibratory Forces Acting on the Surface of a Ship Stern," Trans. SNAME, 1974.

2. S. Tsakonas, J. Breslin, and M. Miller, "Correlation and Application of an Unsteady Flow Theory for Propeller Forces," Trans. SNAME, 1967.

3. J.P. Breslin, "A Theory for the Vibratory Effects Produced by a Propeller on a Large Plate," Journal of Ship Research,

Vol. 3, No. 4, December 1959.

4. J.P. Breslin, "A Theory for the
    Vibratory Forces on a Flat Plate
    Arising From Intermittent Pro-
    peller Blade Cavitation," Sympo-
    sium on Hydrodynamics of Ship and
    Off Shore Propulsions Systems,
    Oslo, Norway, March 1977.

5. W. Vorus, S. Stiansen, and R. Bertz,
    "Correlations or Propeller Induced
    Forces and Structural Vibratory
    Response of the M.V. Roger Blough,"
    The University of Michigan, Dept.
    of Naval Architecture and Marine
    Engineering, Report No. 193A,
    April, 1978.

6. W.S. Vorus, "Calculation of Pro-
    peller Induced Forces, Force
    Distributions, and Pressures;
    Free-Surface Effects," Journal of
    Ship Research, Vol. 28, No. 2,
    June 1976.

7. W.S. Vorus, "An Integrated Approach
    to the Determination of Propeller
    Generated Vibratory Forces Acting
    on a Ship Hull," The University of
    Michigan, Dept. of Naval Architec-
    ture and Marine Engineering,
    Report No. 072, 1971.

8. M.M. Sluyter, "A Computational
    Program and Extended Tabulation
    of Legendre Functions of the
    Second Kind and Half Order,"
    Therm Advanced Research Report
    TAR-TR601, August 1960.

9. W. Frank, "Oscillations of Cylin-
    ders in or Below the Free Sur-
    face of Deep Fluids," Naval Ship
    Research and Development Center
    Report No. 2375, Washington, DC,
    1967.

10. J.L. Hess, and A. Smith, "Calcula-
    tion of Non-Lifting Potential
    Flow About Arbitrary Three-Dimen-
    sional Bodies," Douglas Aircraft
    Corporation Report No. ES 40622,
    March 1962.

APPENDIX

GENERALIZATION AND COMPUTATIONAL IMPROVE-
MENT OF THE HULL SURFACE FORCE FORMULA

FORMULA GENERALIZATION

A formula for calculating the
complex amplitude of the nth blade-rate
harmonic of the propeller-induced hull
surface force in direction i was origi-
nally derived in reference [7] as,

$$F_{in} = \frac{N\omega}{\pi} \int_{\pi/N\omega}^{\pi/N\omega} e^{-inN\omega t} \int\int \left[\frac{\mu(R_1)}{U} \int_{P(\vec{R}_1)}^{\infty} e^{inN\frac{\omega}{U}(x_1-\xi)} \vec{n}_p \right.$$

$$\left. \cdot \vec{\nabla} H_{in}(\vec{R}_1) d\xi - \rho q(\vec{R}_1) H_{in}(\vec{R}_1) \right] dSdt \qquad (28)$$

Here the propeller is represented in
terms of singularity distributions $\mu(\vec{R}_1)$
and $q(\vec{R}_1)$. $\mu(\vec{R}_1)$ is a distribution of
normal dipoles over the blade pitch
surfaces and their helicoidal extensions
downstream; $\mu(\vec{R}_1)$ represents the un-
steady lifting effects of the propeller
blades. $q(\vec{R}_1)$ is a distribution of
sources over the blade pitch surfaces
and represents the thickness effects of
the propeller blades.

The source representation for blade
thickness is disadvantageous from a
computational point of view. Chordwise
rates of change of blade thickness are
required in the construction of $q(\vec{R}_1)$.
While the blade thickness distribution
is always specified on the propeller
drawing, its chordwise rates of change
are troublesome to estimate, particular-
ly near the chordwise extremities. More
importantly, when blade cavitation
occurs, it is useful to simply consider
the blade as having a time-dependent
thickness distribution composed of the
thickness of the blade proper plus that
of the attached cavitation. While an
approximate cavity thickness distribu-
tion might be estimated from, say,
observations or photographs of cavita-
tion tests, it is unlikely that such
could lead to usefully accurate esti-
mates of the rates of change of cavity
thickness required in the construction
of $q(\vec{R}_1)$ in (28).

These problems associated with the
rate of change of blade thickness can
be overcome by using a tangential dipole
distribution, instead of a source dis-
tribution, to represent the effects of
blade thickness in the hull surface
force calculation. The tangential
dipole singularity, being of higher
order than the source, requires the
thickness distribution itself, rather
than the distribution of thickness
derivative, in its construction. In
view of the advantage of tangential
dipoles over sources, the hull-surface
force formula, (28), was rederived in
terms of tangential dipoles directly in
both references [1] and [6]. However,
the tangential dipole form of references
[1] and [6] is not completely general.
That is, in the case of a time-dependent
blade thickness, which corresponds to a
cavitating propeller, tangential dipoles
alone are not sufficient to completely
represent the thickness effect; a line
source along the blade trailing edge,
whose strength at any radius is equal to
the instantaneous time rate of change of
the blade cross-sectional area at that
radius, is required additionally.

A form of the hull-surface force
formula which properly allows for blade
cavitation, while taking advantage of a
tangential dipole distribution for thick-
ness, can be manipulated from (28). Write

F_{in} in (28) as, $F_{in}=F_{in_\ell}+F_{in_t}$ where subscripts ℓ and t denote "lift" and "thickness." The thickness part is isolated as,

$$F_{in_t}=-\frac{\rho N\omega}{\pi}\int\limits_{-\pi/N\omega}^{\pi/N\omega}e^{-inN\omega t}\iint\limits_{P(\vec{R}_1)}q(\vec{R}_1)H_{in}(\vec{R}_1)dSdt \qquad (29)$$

The surface integral in (29) is an integral over all propeller blades; $\vec{R}_1$, the position vector to a blade point, is time-dependent. Write the surface integral in (29) as,

$$\iint\limits_{P(\vec{R}_1)}q(\vec{R}_1)H_{in}(\vec{R}_1)dS$$

$$= \int\limits_{\substack{\text{radially}\\\text{over N}\\\text{blades}}}\int\limits_{LE(r_1)}^{TE(r_1)}q(\ell,r_1,t)H_{in}(\ell,r_1,t)d\ell dr_1$$

The inner line integral in ℓ is along the blade section at radius r_1; refer to Figure 6. Write,

$$I(r_1,t) = \int\limits_{LE(r_1)}^{TE(r_1)}q(\ell,r_1,t)H_{in}(\ell,r_1,t)d\ell \qquad (30)$$
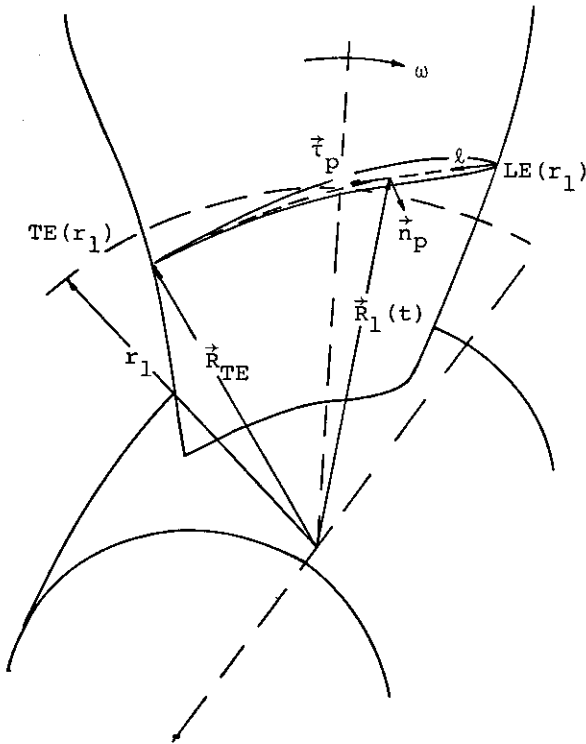
Figure 6. Propeller Geometry

and integrate by parts along the section; the positive ℓ direction is identified by the unit vector $\vec{\tau}_p$ on Figure 6, which is tangent to the section pitch-line at radius r_1.

$$u = H_{in} \qquad\qquad dv = qd\ell$$

$$du=\vec{\nabla}H_{in}\cdot\vec{\tau}_pd\ell \qquad v=\int^\ell q(\zeta,r_1,t)d\zeta$$

Write $v(\ell,r_1,t)$ as,

$$v(\ell,r_1,t)=v(LE,r_1,t)+\int\limits_{\zeta=LE}^\ell q(\zeta,r_1,t)d\zeta$$

and define,

$$\sigma(\ell,r_1,t)=\int\limits_{\zeta=LE}^\ell q(\zeta,r_1,t)d\zeta \qquad (31)$$

Then I, from (30), is,

$$I=H_{in}(\ell,r_1,t)v(LE,r_1,t)\Big|_{LE}^{TE}$$

$$+H_{in}(\ell,r_1,t)\sigma(\ell,r_1,t)\Big|_{LE}^{TE} \qquad (32)$$

$$-\int\limits_{LE}^{TE}v(LE,r_1,t)\vec{\nabla}H_{in}\cdot\vec{\tau}_pd\ell-\int\limits_{LE}^{TE}\sigma(\ell,r_1,t)\vec{\nabla}H_{in}\cdot\vec{\tau}_pd\ell$$

The first and third terms in (32) cancel identically. $\sigma(LE,r_1,t)=0$ by (31). (32) then becomes,

$$I = H_{in}(TE,r_1,t)\sigma(TE,r_1,t)$$

$$-\int\limits_{\zeta=LE}^{TE}\sigma(\ell,r_1,t)\vec{\nabla}H_{in}\cdot\vec{\tau}_pd\ell$$

By (31),

$$\sigma(TE,r_1,t) = \int\limits_{\zeta=LE}^{TE}q(\zeta,r_1,t)d\ell \qquad (31.1)$$

which is just the net source strength of the blade section at r_1, at time t. Denote, $\sigma(TE,r_1,t)=Q(r_1,t)$. The surface force due to blade thickness is then obtained by substitution back in (29),

$$F_{in_t}=\frac{\rho N\omega}{\pi}\int\limits_{-\pi/N\omega}^{\pi/N\omega}e^{-inN\omega t}\left[\iint\limits_{P(\vec{R}_1)}\sigma(\vec{R}_1)\vec{\nabla}H_{in}(\vec{R}_1)\cdot\vec{\tau}_pdS\right.$$

$$\left.-\int\limits_{TE(\vec{R}_{TE})}Q(\vec{R}_{TE})H_{in}(\vec{R}_{TE})ds\right] dt$$

Here, $\vec{R}_{TE}$ is vector position to the blade trailing edges.

The complete force, corresponding to (28), is therefore,

$$F_{in} = \frac{N\omega}{\pi} \int_{-\pi/N\omega}^{\pi/N\omega} e^{-inN\omega t} \left\{ \iint_{P(\vec{R}_1)} \left[\frac{\mu(\vec{R}_1)}{U} \int_{\xi=x_1}^{\infty} d\xi e^{inN\frac{\omega}{U}(x_1-\xi)} \frac{\partial}{\partial n_p} \right. \right.$$

$$\left. + \rho\sigma(\vec{R}_1) \frac{\partial}{\partial \tau_p} \right] H_{in}(R_1) dS \qquad (33)$$

$$\left. - \rho \int_{TE(\vec{R}_{TE})} \mathcal{Q}(\vec{R}_{TE}) H_{in}(\vec{R}_{TE}) dS \right\} dt$$

The first two terms in (33) correspond to the formula derived in [1] and [6]. $\sigma(\vec{R}_1)$ represents a distribution of tangential dipoles over the blade pitch surfaces; the axis of the dipoles is $\vec{\tau}_p$. The third term in (33) represents the contribution from a line source along the blade trailing edges; the strength of the line source is equal to the dipole density at the trailing edge, $\sigma(\vec{R}_{TE})$, by (31.1). $\sigma(\vec{R}_{TE})$, and therefore the third term in (33), will be zero when the blade thickness is time invariant (non-cavitating blades). For the cavitating blade, the line-source will contribute.

FORMULA REORGANIZATION

Formula (33) can be reorganized for computational advantage. First make the change of variable,

$$\theta = \omega t$$

θ is the positive counterclockwise looking forward (so that, for right hand rotation, ω is negative). Also write, $H_{in}(\vec{R}_1) = inN\omega\phi_i(\vec{R}_1)$ so that, in view of the definition of H_{in}, ϕ_i becomes the potential due to the hull moving steadily with unit velocity in direction i through the fluid (the subscript i denotes direction; the factor $i=\sqrt{-1}$). (33) can be rewritten as,

$$F_{in} = \frac{inN^2\omega}{\pi} \int_{-\pi/N}^{\pi/N} e^{-inN\theta} \left\{ \iint_{P(\vec{R}_1)} \left[\rho\sigma(\vec{R}_1)\vec{\tau}_p \right. \right.$$

$$\left. + \frac{1}{U}\mu(\vec{R}_1)\vec{n}_p \int_{\xi=x_1}^{\infty} d\xi e^{inN\frac{\omega}{U}(x_1-\xi)} \right] \cdot \vec{\nabla}\phi_i(\vec{R}_1) dS$$

$$\left. - \rho \int_{TE(\vec{R}_{TE})} \mathcal{Q}(\vec{R}_{TE})\phi_i(\vec{R}_{TE}) dS \right\} d\theta \qquad (34)$$

In this form the slip-stream integral in ξ is to be interpreted as an operator on $\vec{\nabla}\phi_i(\vec{R}_1)$ with x_1 and $\vec{R}_1$ replaced by ξ. The position vector $\vec{R}_1$ to a point on the kth blade, $k=0,\ldots N-1$, can be written

$$\vec{R}_1 = x_1\vec{i} + r_1\vec{e}_r + r_1\theta_1\vec{e}_\theta$$

in a coordinate system fixed in space at the propeller hub; see Figure 7.

By inspection of the limits on the θ integral in (34), θ is the position angle to the generator line of the blade nearest top-dead-center (k=0). Therefore, if $\vec{R}_1$ is a point on the kth blade, θ_1, in $\vec{R}_1$, is

$$\theta_1 = \theta + \frac{2\pi k}{N} + \alpha \qquad (35)$$

where α is the position angle in the projected plane to $\vec{R}_1$ relative to the kth blade generator line, as indicated on Figure 7.
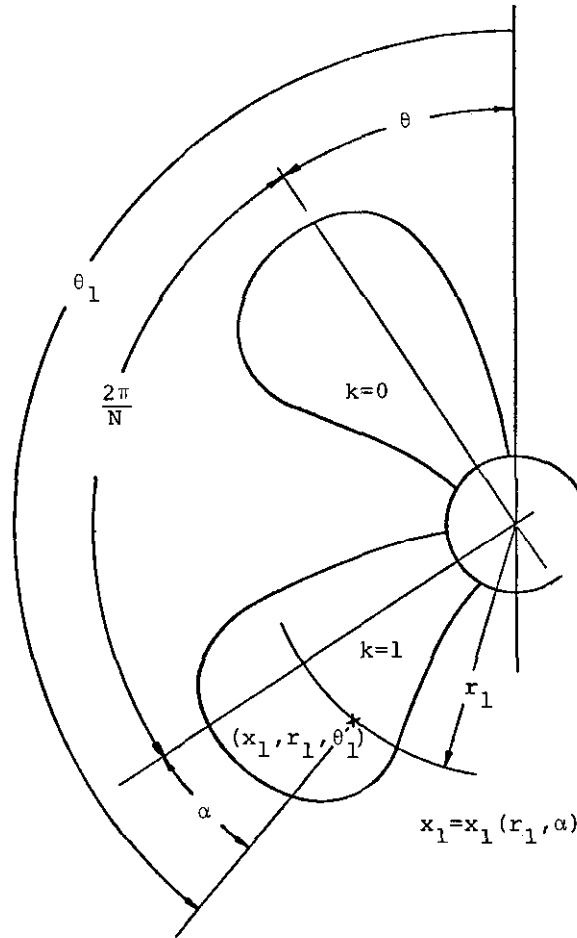

Figure 7. Propeller Coordinates

Now write σ, μ, ϕ_i, and $\vec{\nabla}\phi_i$ as Fourier series in the angular coordinates as follows:

$$\mu(r_1,\alpha,x_1,\theta,k) = \mathrm{Re} \sum_{m=0}^{\infty} \mu_m(r_1,\theta) e^{im(\theta+\frac{2\pi k}{N})} \qquad (36)$$

$$\sigma(r_1,\alpha,x_1,\theta,k) = \mathrm{Re} \sum_{m=0}^{\infty} \sigma_m(r_1,\alpha) e^{im(\theta+\frac{2\pi k}{N})} \qquad (37)$$

$$\vec{\nabla}\phi_i(r_1,\alpha,x_1,\theta,k) \equiv \vec{v}_i(r_1,\alpha,x_1,\theta,k) = \mathrm{Re} \sum_{\nu=0}^{\infty} \vec{v}_{i\nu}(r_1,x_1) e^{i\nu(\theta+\frac{2\pi k}{N}+\alpha)} \qquad (38)$$

$$\phi_i(r_1,\alpha,x_1,\theta,k) = \mathrm{Re} \sum_{\nu=0}^{\infty} \phi_{i\nu}(r_1,x_1) e^{i\nu(\theta+\frac{2\pi k}{N}+\alpha)} \qquad (39)$$

x_1 is deleted from the argument lists in μ_m and σ_m since, on the blade, x_1 is a function of α.

Now substitute (36) through (39) into (34) and replace the N-blade integration over $P(\vec{R}_1)$ by an integration over the index blade (k=0) and a summation over k. The result is,

$$F_{in} = \frac{inN^2\omega}{\pi} \int_{-\pi/N}^{\pi/N} d\theta\, e^{-inN\theta} \sum_{k=0}^{N-1} \left\{ \iint_{B(r_1,\alpha)} \mathrm{Re} \sum_{m=0}^{\infty} \left[\rho\sigma_m \vec{\tau}_p \right. \right.$$

$$+ \frac{1}{U}\mu_m \vec{n}_p \int_{\xi=x_1}^{\infty} d\xi\, e^{inN\frac{\omega}{U}(x_1-\xi)} \bigg] e^{im(\theta+\frac{2\pi k}{N})}$$

$$\cdot \mathrm{Re} \sum_{\nu=0}^{\infty} \vec{v}_{i\nu}(r_1,x_1) e^{i\nu(\theta+\frac{2\pi k}{N}+\alpha)} dS$$

$$- \rho \int_{r_1=r_h}^{r_t} \mathrm{Re} \sum_{m=0}^{\infty} Q_m(r_1) e^{im(\theta+\frac{2\pi k}{N})}$$

$$\cdot \mathrm{Re} \sum_{\nu=0}^{\infty} \phi_{i\nu}(r_1,x_{1_t})$$

$$\left. \left. \cdot e^{i\nu(\theta+\frac{2\pi k}{N}+\alpha_t)} dr_1 \right\} \qquad (40) \right.$$

In (40),
$Q_m(r_1) = \sigma_m(r_1,\alpha_t)$ by (31.1), where $\alpha_t = \alpha_t(r_1)$ is the projected trailing edge angle of the index (k=0) blade at radius r_1. Also, $x_{1_t} \equiv x_1(r_1,\alpha_t)$ in the last term in (40). Temporarily define,

$$\vec{S}_m(r_1,\alpha) \equiv \rho\sigma_m(r_1,\alpha)\vec{\tau}_p(r_1)$$

$$+ \frac{1}{U}\mu_m(r_1,\alpha)\vec{n}_p(r_1) \int_{\xi=x_1}^{\infty} d\xi\, e^{inN\frac{\omega}{U}(x_1-\xi)}$$

keeping in mind that the ξ integral in $\vec{S}_m$ is an operator on $\vec{v}_{i\nu}(r_1,x_1)$ with $x_1=\xi$. (40) can then be written,

$$F_{in} = \frac{inN^2\omega}{\pi} \int_{-\pi/N}^{\pi/N} e^{-inN\theta} \left[\iint_{B(r_1,\alpha)} \sum_{k=0}^{N-1} \left\{ \frac{1}{2}\sum_{m=0}^{\infty} \left[\vec{S}_m e^{im(\theta+\frac{2\pi k}{N})} \right. \right. \right.$$

$$\left. + \vec{\bar{S}}_m e^{-im(\theta+\frac{2\pi k}{N})} \right] \cdot \frac{1}{2} \sum_{\nu=0}^{\infty} \left[\vec{v}_{i\nu} e^{i\nu(\theta+\frac{2\pi k}{N}+\alpha)} \right.$$

$$\left. \left. + \vec{\bar{v}}_{i\nu} e^{-i\nu(\theta+\frac{2\pi k}{N}+\alpha)} \right] \right\} dS \qquad (41)$$

$$- \rho \int_{r_1=r_h}^{r_t} \sum_{k=0}^{N-1} \left\{ \frac{1}{2}\sum_{m=0}^{\infty} \left[Q_m e^{im(\theta+\frac{2\pi k}{N})} + \bar{Q}_m e^{-im(\theta+\frac{2\pi k}{N})} \right] \right.$$

$$\cdot \frac{1}{2}\sum_{\nu=0}^{\infty} \left[\phi_{i\nu} e^{i\nu(\theta+\frac{2\pi k}{N}+\alpha_t)} \right.$$

$$\left. \left. + \bar{\phi}_{i\nu} e^{-i\nu(\theta+\frac{2\pi k}{N}+\alpha_t)} \right] \right\} dr_1 \bigg] d\theta$$

where the "barred" terms in (41) represent the respective complex conjugates.

Performing the multiplications and interchanging the order of summation in (41) gives,

$$F_{in} = \frac{inN^2\omega}{\pi} \int_{-\pi/N}^{\pi/N} e^{-inN\theta} \left[\iint_{B(r_1,\alpha)} \sum_{m=0}^{\infty} \sum_{\nu=0}^{\infty} \right.$$

$$\cdot \left\{ \vec{S}_m \cdot \vec{v}_{i\nu} e^{i\nu\alpha} e^{i\theta(\nu+m)} \sum_{k=0}^{N-1} e^{i(\nu+m)\frac{2\pi k}{N}} \right.$$

$$+ \vec{\bar{S}}_m \cdot \vec{v}_{i\nu} e^{i\nu\alpha} e^{i\theta(\nu-m)} \sum_{k=0}^{N-1} e^{i(\nu-m)\frac{2\pi k}{N}}$$

$$+ \vec{S}_m \cdot \vec{\bar{v}}_{i\nu} e^{-i\nu\alpha} e^{-i\theta(\nu-m)} \sum_{k=0}^{N-1} e^{-i(\nu-m)\frac{2\pi k}{N}}$$

$$\qquad (42)$$

$$\left. + \vec{\bar{S}}_m \cdot \vec{\bar{v}}_{i\nu} e^{-i\nu\alpha} e^{-i\theta(\nu+m)} \sum_{k=0}^{N-1} e^{-i(\nu+m)\frac{2\pi k}{N}} \right\} dS$$

$$- \rho \int_{r_1=r_h}^{r_t} \sum_{m=0}^{\infty} \sum_{\nu=0}^{\infty} Q_m \phi_{i\nu} e^{i\nu\alpha_t} e^{i\theta(\nu+m)} \sum_{k=0}^{N-1} e^{i(\nu+m)\frac{2\pi k}{N}}$$

$$+\bar{Q}_m\phi_{i\nu}e^{i\nu\alpha_t}e^{i\theta(\nu-m)}\sum_{k=0}^{N-1}e^{i(\nu-m)\frac{2\pi k}{N}}$$

$$+Q_m\bar{\phi}_{i\nu}e^{-i\nu\alpha_t}e^{-i\theta(\nu-m)}\sum_{k=0}^{N-1}e^{-i(\nu-m)\frac{2\pi k}{N}}$$

$$+\bar{Q}_m\bar{\phi}_{i\nu}e^{-i\nu\alpha_t}e^{-i\theta(\nu+m)}\ .$$

$$\cdot\sum_{k=0}^{N-1}e^{-i(\nu+m)\frac{2\pi k}{N}}\Bigg\}dr_1\Bigg]d\theta$$

If the integration order is likewise interchanged in (42), four terms of the following type will occur,

$$\int_{-\pi/N}^{\pi/N}e^{i\theta(\beta-nN)}d\theta\ \cdot\ \sum_{k=0}^{N-1}e^{\frac{2\pi i\beta k}{N}}$$

where β represents the linear combinations of ν and m. Since ν and m are both integers, β is an integer. Therefore,

$$\int_{-\pi/N}^{\pi/N}e^{i\theta(\beta-nN)}d\theta=\begin{cases}\dfrac{2\pi}{N} & \beta=nN\\[2ex]0 & \beta\neq nN\end{cases}$$

Then, for $\beta=nN$

$$\sum_{k=0}^{N-1}e^{2\pi ink}=N$$

The four β expressions then define four relationships between the m and ν. For the first and fifth in (42),

$\beta=\nu+m=nN$ implies $m=nN-\nu$

Then, since $m\geq0$ and $\nu\geq0$,

$\nu=0,1,\ldots nN$

Likewise for the other three β's:

$\beta=\nu-m=nN$ $\qquad$ $m=\nu-nN\geq0$
$\qquad\qquad\qquad\qquad\qquad\quad$ $\nu=nN,\ldots\infty$

$\beta=-\nu+m=nN$ $\qquad$ $m=nN+\nu$
$\qquad\qquad\qquad\qquad\qquad\quad$ $\nu=0,\ldots\infty$

In the fourth and last terms, $\beta=-\nu-m$. With m and $\nu\geq0$, $-\nu-m\neq nN$ unless $n=0$ and $\nu=m=0$. But $n>0$ because of the unsteadiness, so the fourth and eighth terms in (42) are zero for all ν and m.
   Making these substitutions, (42) reduces to:

$$F_{in}=\frac{inN^2\omega}{2}\Bigg[\iint_{B(r_1,\alpha)}\Bigg\{\sum_{\nu=0}^{nN}\vec{S}_{nN-\nu}\cdot\vec{v}_{i\nu}e^{-i\nu\alpha}$$

$$+\sum_{\nu=nN}^{\infty}\vec{\bar{S}}_{\nu-nN}\cdot\vec{v}_{i\nu}e^{i\nu\alpha}+\sum_{\nu=0}^{\infty}\vec{\bar{S}}_{\nu+nN}\cdot\vec{\bar{v}}_{i\nu}e^{-i\nu\alpha}\Bigg\}dS$$

$$-\rho\int_{r_1=r_h}^{r_t}\Bigg\{\sum_{\nu=0}^{nN}Q_{nN-\nu}\phi_{i\nu}e^{i\nu\alpha_t}\qquad\qquad(43)$$

$$+\sum_{\nu=nN}^{\infty}\bar{Q}_{\nu-nN}\phi_{i\nu}e^{i\nu\alpha_t}\ +$$

$$+\sum_{\nu=0}^{\infty}Q_{\nu+nN}\bar{\phi}_{i\nu}e^{-i\nu\alpha_t}\Bigg\}dr_1\Bigg]$$

The blade integral in (43) can be written explicitly as,

$$\iint_{B(r_1,\alpha)}dS\equiv\int_{r_1=r_h}^{r_t}\frac{r_1}{\cos\beta(r_1)}\int_{\alpha=\alpha_\ell(r_1)}^{\alpha_t(r_1)}d\alpha dr_1$$

where r_h and r_t are the hub and tip radii, respectively and α_ℓ and α_t are the projected leading and trailing edge angles, relative to the generator line of the blade section at r_1 (see Figure 8). $\beta(r_1)$ is the geometric pitch angle. Also referring to Figure 8,

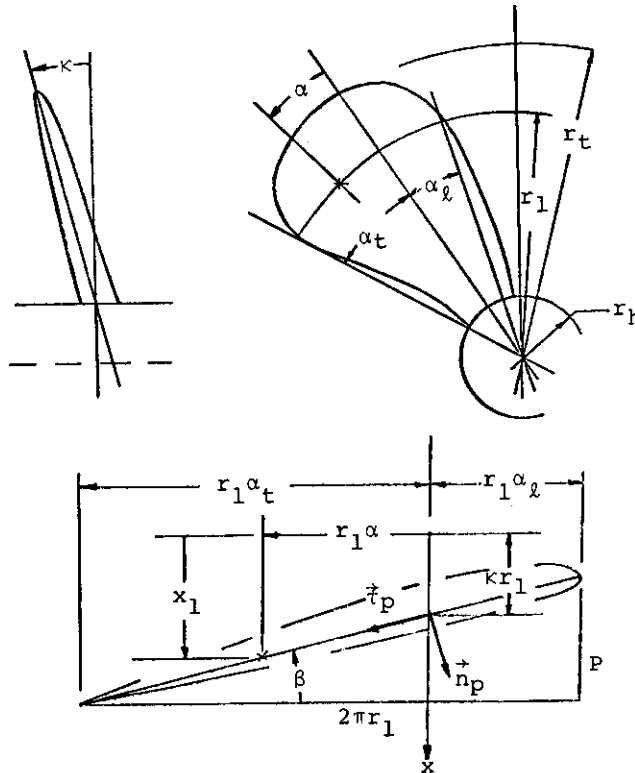Figure 8. Propeller Blade Geometry

$$\vec{n}_p = \frac{2\pi r_1 \vec{i} - 2\pi r_1 \kappa \vec{e}_r - P\vec{e}_\theta}{\sqrt{4\pi^2 r_1^2 (1+\kappa^2) + P^2}} \qquad (44)$$

and

$$\vec{\tau}_p = \frac{P\vec{i} + 2\pi r_1 \vec{e}_\theta}{\sqrt{4\pi^2 r_1^2 + P^2}} \qquad (45)$$

where $P(r_1)$ is the section geometric pitch.

An approximation can be made at this point which substantially simplifies (43). Note that $\vec{v}_{i\nu}$, and the integral operator on $\vec{v}_{i\nu}$ in $\vec{S}_m$, depend on α only through x_1.

$$x_1 = x_1(r_1, \alpha) = r_1[\kappa + \alpha \tan\beta(r_1)]$$

Referring to Figure 8, κ is the blade rake angle and $\beta(r_1)$ is the section pitch angle. β is small, at least near the blade tip; the blade tip region is predominately influential in the vibratory force. Therefore, x_1 can be replaced approximately by its value at the generator line.

$$x_1(r_1, \alpha) \simeq x_1(r_1) \simeq \kappa r_1 \text{ also small.}$$

$$(46)$$

The product $\vec{S}_m \cdot \vec{v}_{i\nu}$ then becomes,

$$\vec{S}_m \cdot \vec{v}_{i\nu} = \rho\sigma_m(r_1, \alpha) \vec{\tau}_p(r_1) \cdot \vec{v}_{i\nu}(r_1)$$

$$+ \frac{1}{U}\mu_m(r_1, \alpha) \vec{n}_p(r_1) \cdot \int_{\xi = x_1(r_1)}^\infty e^{inN\frac{\omega}{U}(x_1 - \xi)} \vec{v}_{i\nu}(r_1, \xi) d\xi$$

and likewise for the respective conjugate combinations. The only dependency on α in any of these terms is through the σ_m and μ_m. Define the following:

$$T_{nN-\nu}(r_1) \equiv \frac{r_1}{\cos\beta} \int_{\alpha = \alpha_\ell}^{\alpha_t} \sigma_{nN-\nu}(r_1, \alpha) e^{i\nu\alpha} d\alpha$$

$$T_{\nu-nN}(r_1) \equiv \frac{r_1}{\cos\beta} \int_{\alpha = \alpha_\ell}^{\alpha_t} \bar{\sigma}_{\nu-nN}(r_1, \alpha) e^{i\nu\alpha} d\alpha$$

$$(47)$$

$$T_{\nu+nN}(r_1) \equiv \frac{r_1}{\cos\beta} \int_{\alpha = \alpha_\ell}^{\alpha_t} \sigma_{\nu+nN}(r_1, \alpha) e^{-i\nu\alpha} d\alpha$$

also,

$$L_{nN-\nu}(r_1) \equiv \frac{r_1}{\cos\beta} \int_{\alpha = \alpha_\ell}^{\alpha_t} \mu_{nN-\nu}(r_1, \alpha) e^{i\nu\alpha} d\alpha$$

$$L_{\nu-nN}(r_1) \equiv \frac{r_1}{\cos\beta} \int_{\alpha = \alpha_\ell}^{\alpha_t} \mu_{nN-\nu}(r_1, \alpha) e^{i\nu\alpha} d\alpha$$

$$(48)$$

$$L_{\nu+nN}(r_1) \equiv \frac{r_1}{\cos\beta} \int_{\alpha = \alpha_\ell}^{\alpha_t} \mu_{\nu+nN}(r_1, \alpha) e^{-i\nu\alpha} d\alpha$$

Furthermore, define,

$$\vec{V}_{i\nu}(r_1) \equiv \frac{1}{U} \int_{\xi = x_1(r_1)}^\infty e^{inN\frac{\omega}{U}(x-\xi)} \vec{v}_{i\nu}(r_1, \xi) d\xi \qquad (49)$$

Then, F_{in} from (43), using (47), (48), and (49) becomes,

$$F_{in} = \frac{inN^2\omega}{2} \int_{r_1 = r_h}^{r_t} \left[\sum_{\nu=0}^{-nN} (L_{nN-\nu}\vec{n}_p \cdot \vec{V}_{i\nu} + \rho T_{nN-\nu}\vec{\tau}_p \cdot \vec{v}_{i\nu} \right.$$

$$- \rho Q_{nN-\nu}\phi_{i\nu}e^{i\nu\alpha_t}) + \sum_{\nu=nN}^\infty (L_{\nu-nN}\vec{n}_p \cdot \vec{V}_{i\nu}$$

$$+ \rho T_{\nu-nN}\vec{\tau}_p \cdot \vec{v}_{i\nu} - \rho Q_{\nu-nN}\phi_{i\nu}e^{i\nu\alpha_t}) \qquad (50)$$

$$+ \sum_{\nu=0}^\infty (L_{\nu+nN}\vec{n}_p \cdot \vec{V}_{i\nu} + \rho T_{\nu+nN}\vec{\tau}_p \cdot \vec{v}_i$$

$$\left. - \rho Q_{\nu+nN}\phi_{i\nu}e^{-i\nu\alpha_t}) \right] dr_1$$

(50) is the basic form desired.

While a substantial rearrangement of (33) has been accomplished in (50), it is not immediately obvious that (50) is any better suited for computations than (33).

The predominant expenditure in computing with (33) is the evaluation of $\vec{\nabla}H_{in}(\vec{R}_1) = inN\omega\vec{v}_i(\vec{R}_1)$ at all the quadrature points involved in the triple (thickness) and quadruple (lifting) integrals. If the Fourier analysis of $\vec{v}_i$, to produce the $\vec{v}_{i\nu}$ in (50), was carried out numerically, then the double and triple integrals plus the summation in (50) would replace the triple and quadruple integrals in (33); the two would probably be marginally different from the point of view of computational effort. Fortunately, the Fourier analysis of $\vec{v}_i(\vec{R}_1)$ does not have to be performed numerically.

The major advantage of (50) over (33) is that the Fourier analysis of $\vec{v}_i$ to produce the $\vec{v}_{i\nu}$ can be accomplished analytically. Therefore, (50) becomes an improvement over (33) by the equivalent of one integral order, more or less, when the analytically evaluated $\vec{v}_{i\nu}$ are inserted.

FOURIER ANALYSIS OF THE HULL INDUCED VELOCITY FIELD

The hull-induced velocity potential field, $\phi_i(\vec{R})$, in a coordinate system moving steadily with the hull at unit velocity in direction i, through the ideal fluid, can be written,

$$\phi_i(\vec{R}) = \iint\limits_{S^*(\vec{R}_o)} \sigma_i(\vec{R}_o) \, G(\vec{R};\vec{R}_o) dS \qquad (51)$$

Here $\sigma_i(\vec{R}_o)$ is a source density distribution on the "double hull" surface, $S^*(\vec{R}_o)$; σ_i corresponds to the mode of hull motion, i (direction of force). $S^*(\vec{R}_o)$ is the wetted surface of the bare hull, plus its image in the upper half-space; $\vec{R}_o$ is the position vector to points of the "double-hull" surface. $G(\vec{R},\vec{R}_o) = -\frac{1}{4\pi}\frac{1}{|\vec{R}-\vec{R}_o|}$, the infinite fluid Green's function.

The "double hull" and infinite fluid Green's function representations are permitted by the condition of zero potential on the water free-surface, [7], [1], and [6].

The evaluation of $\phi_i(\vec{R})$ on the propeller blades $\vec{R}=\vec{R}_1=x_1\vec{i}+r_1\vec{e}_r+r_1\theta_1\vec{e}_\theta$ can be expanded in a Fourier series in the angular coordinate θ_1 (see (39) and Figure 9).

$$\phi_i(\vec{R})=\phi_i(x_1,r_1,\theta_1)=\text{Re}\sum_{\nu=0}^\infty \phi_{i\nu}(x_1,r_1)e^{i\nu\theta_1} \qquad (52)$$

with $x_1=\kappa r_1$ by (46).

The hull-induced velocity is,

$$\vec{v}_i(\vec{R}_1) = \vec{\nabla}\phi_i(\vec{R}_1)$$

with $\vec{\nabla}=\frac{\partial}{\partial x_1}\vec{i} + \frac{\partial}{\partial r_1}\vec{e}_r + \frac{1}{r_1}\frac{\partial}{\partial\theta_1}\vec{e}_\theta \qquad (53)$

Therefore, by (52),

$$\vec{v}_i(\vec{R}_1) = \text{Re}\sum_{\nu=0}^\infty \vec{\nabla}[\phi_{i\nu}(x_1,r_1)e^{i\nu\theta_1}]$$

Applying (53) gives,

$$\vec{v}_i(\vec{R}_1)=\text{Re}\sum_{\nu=0}^\infty\left[\frac{\partial\phi_{i\nu}}{\partial x_1}\vec{i}+\frac{\partial\phi_{i\nu}}{\partial r_1}\vec{e}_r+\frac{i\nu}{r_1}\phi_{i\nu}\vec{e}_\theta\right]e^{i\nu\theta_1} \qquad (54)$$

With $\theta_1=\theta+\frac{2\pi k}{N}+\alpha$ from (35) and Figure 7, the Fourier series of $\vec{v}_i$ from (38) can be written,

$$\vec{v}_i(\vec{R}_1)=\text{Re}\sum_{\nu=0}^\infty\vec{v}_{i\nu}(r_1,x_1)e^{i\nu\theta_1} \qquad (55)$$

Comparison of (54) and (55) implies,

$$\vec{v}_{i\nu}=\frac{\partial\phi_{i\nu}}{\partial x_1}\vec{i} +\frac{\partial\phi_{i\nu}}{\partial r_1}\vec{e}_r + \frac{i\nu}{r_1}\phi_{i\nu}\vec{e}_\theta \qquad (56)$$

With $\vec{n}_p$ and $\vec{\tau}_p$ in (50) given as (34) and (35), the dot product is clear; it is only necessary to determine the $\phi_{i\nu}$. (52) implies,

$$\phi_{i\nu}(x_1,r_1)=\frac{\varepsilon_o}{\pi}\int_{\theta_1=-\pi}^\pi \phi_i(x_1,r_1,\theta_1)e^{-i\nu\theta_1}\,d\theta_1 \qquad (57)$$

where $\varepsilon_o = \begin{cases} \frac{1}{2} & \nu = 0 \\ 1 & \nu > 0 \end{cases}$

Let $\vec{R}=\vec{R}_1$ in (51) and substitute into (57)

$$\phi_{i\nu}(x_1,r_1)$$

$$=\frac{\varepsilon_o}{\pi}\int_{-\pi}^\pi\iint\limits_{S^*(\vec{R}_o)}\sigma_i(\vec{R}_o)G(\vec{R}_1;\vec{R}_o)dSe^{-i\nu\theta_1}\,d\theta_1$$

Interchanging the order of integration,

$$\phi_{i\nu}(x_1,r_1)$$

$$=\iint\limits_{S^*(\vec{R}_o)}\sigma_i(\vec{R}_o)\frac{\varepsilon_o}{\pi}\int_{\theta_1=-\pi}^\pi G(\vec{R}_1;\vec{R}_o)e^{-i\nu\theta_1}\,d\theta_1 dS$$
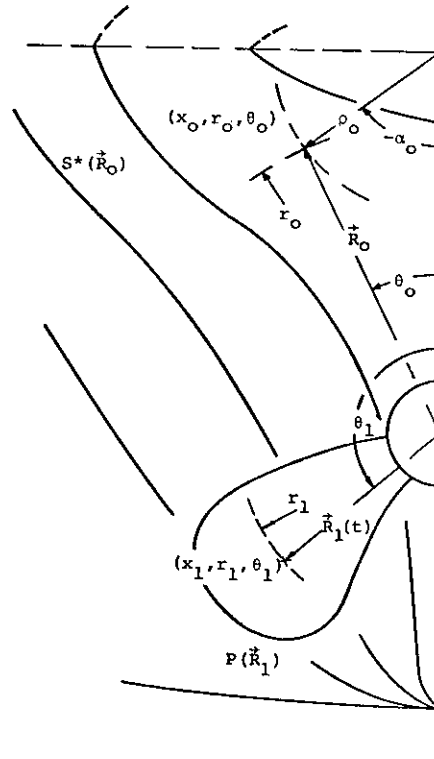

Figure 9. Hull/Propeller Coordinates

Define,

$$G_\nu(x_1, r_1; \vec{R}_o) = \frac{\varepsilon_o}{\pi} \int_{\theta_1 = -\pi}^{\pi} G(x_1, r_1, \theta_1; \vec{R}_o) e^{-i\nu\theta_1} d\theta_1 \qquad (58)$$

which is just the νth Fourier coefficient of G. Then,

$$\phi_{i\nu}(x_1, r_1) = \int\int_{S*(\vec{R}_o)} \sigma_i(\vec{R}_o) G_\nu(x_1, r_1; \vec{R}_o) dS \qquad (59)$$

Now, considering (58), let $\vec{R}_o$ be,

$$\vec{R}_o = x_o \vec{i} + r_o \vec{e}_r + r_o \theta_o \vec{e}_\theta$$

where (x_o, r_o, θ_o) is a point on the "double hull" surface in the coordinate system fixed at the propeller hub (see Figure 9). $G(\vec{R}_1; \vec{R}_o)$ in this coordinate system can be written,

$$G(R_1; R_o) =$$

$$-\frac{1}{4\pi} \frac{1}{\sqrt{(x_1 - x_o)^2 + r_1^2 + r_o^2 - 2r_1 r_o \cos(\theta_1 - \theta_o)}}$$

This function has the following representation in terms of the Legendre function of the second kind of half-integer order,

$$G(R_1; R_o) = -\frac{1}{4\pi} \frac{1}{\sqrt{r_1 r_o}} \cdot$$

$$\cdot \sum_{m=-\infty}^{\infty} Q_{m-1/2}\left[\frac{(x_1-x_o)^2 + r_1^2 + r_o^2}{2r_1 r_o}\right] e^{im(\theta_1 - \theta_o)} \qquad (60)$$

Substitute (60) into (58) and interchange the order of summation and integration

$$G_\nu = -\frac{\varepsilon_o}{4\pi^3} \frac{1}{\sqrt{r_1 r_o}} \sum_{m=-\infty}^{\infty} Q_{m-1/2}\left[\frac{(x_1-x_o)^2 + r_1^2 + r_o^2}{2r_1 r_o}\right]$$

$$e^{-im\theta_o} \int_{\theta_1=-\pi}^{\pi} e^{i(m-\nu)\theta_1} d\theta_1 \qquad (61)$$

But

$$\int_{-\pi}^{\pi} e^{i(m-\nu)\theta_1} d\theta_1 = \begin{cases} 0 & m \neq \nu \\ 2\pi & m = \nu \end{cases}$$

(61) therefore becomes,

$$G_\nu(x_1, r_1; R_o) = -\frac{\varepsilon_o}{2\pi^2} \frac{1}{\sqrt{r_1 r_o}} \cdot$$

$$e^{-i\nu\theta_o} Q_{\nu-1/2}\left[\frac{(x_1-x_o)^2 + r_1^2 + r_o^2}{2r_1 r_o}\right] \qquad (62)$$

(62) substituted into (59), and with this result substituted into (56), gives the $\phi_{i\nu}$ and the $\vec{v}_{i\nu}$ for use in (50). The hull source density, $\sigma_i(R_o)$ and the propeller dipole strength harmonics, $\sigma_m(r_1, \alpha)$ and $\mu_m(r_1, \alpha)$, only remain to be specified.

HIGH FREQUENCY APPROXIMATION

One further approximation with regard to (50) will be valid in most cases. Reconsider (49),

$$V_{i\nu}(r_1) = \frac{1}{U} \int_{\xi=x_1(r_1)}^{\infty} e^{inN\frac{\omega}{U}(x_1-\xi)} \vec{v}_{i\nu}(r_1, \xi) d\xi \qquad (49)$$

If the oscillating exponential varies more rapidly than $\vec{v}_{i\nu}$ in ξ, then the argument of the exponential can be considered as "large," and $\vec{v}_{i\nu}$ can be expanded in an asymptotic series. Assuming this to be the case, the asymptotic expansion of $\vec{V}_{i\nu}$ is obtained from (49) by integration by parts in ξ. Integrating by parts once gives,

$$\vec{V}_{i\nu} = \frac{1}{U}\left\{ -\frac{U}{inN\omega} e^{inN\frac{\omega}{U}(x_1-\xi)} \vec{v}_{i\nu}(r_1, \xi) \Big|_{\xi=x_1}^{\infty} + \frac{U}{inN\omega} \int_{\xi=x_1}^{\infty} e^{inN\frac{\omega}{U}(x_1-\xi)} \frac{\partial}{\partial\xi}\vec{v}_{i\nu}(r_1, \xi) d\xi \right\}$$

For the conditions stated, the remaining integral term is small. Then, to one term,

$$\vec{V}_{i\nu}(r_1) = \frac{1}{inN\omega} \vec{v}_{i\nu}(r_1, x_1)$$

$$= \frac{1}{inN\omega} \vec{v}_{i\nu}(r_1)$$

since $x_1 \approx x_1(r_1) = \kappa r_1$ by (46).
Now before substituting back into F_{in}, (50), define,

$$\vec{K}_m = \rho inN\omega T_m \vec{\tau}_p + L_m \vec{n}_p \qquad (63)$$

With T_m and L_m defined by (47) and (48), (50) may now be written,

$$F_{in} = \frac{N}{2} \int_{r_1=r_h}^{r_t}\left[\sum_{\nu=0}^{nN} (\vec{K}_{nN-\nu} \cdot \vec{v}_{i\nu} - \rho inN\omega Q_{nN-\nu}\phi_{i\nu} e^{i\nu\alpha t})\right.$$

$$+ \sum_{\nu=nN}^{\infty} (\vec{K}_{\nu-nN} \cdot \vec{v}_{i\nu} - \rho i n N \omega Q_{\nu-nN} \phi_{i\nu} e^{i\nu\alpha_t})$$

$$+ \left. \sum_{\nu=0}^{\infty} (\vec{K}_{\nu+nN} \cdot \vec{v}_{i\nu} - \rho i n N \omega Q_{\nu+nN} \bar{\phi}_{i\nu} e^{-i\nu\alpha_t}) \right] dr_1$$

$$(64)$$

(64) will be the preferred form for most all computations of F_{in}.

NUMERICAL ANALYSIS

The potential and velocity induced by the bare hull in the propeller disk are given by (59) and (56) as,

$$\phi_{i\nu}(x_1,r_1) = \int\int_{S*(\vec{R}_0)} \sigma_i(\vec{R}_0) G_\nu(x_1,r_1;\vec{R}_0) dS \quad (59)$$

$$\vec{v}_{i\nu}(x_1,r_1) = \int\int_{S*(R_0)} \sigma_i(\vec{R}_0) \vec{\nabla} G_\nu(x_1,r_1;\vec{R}_0) dS \quad (65)$$

where, by (53),

$$\vec{\nabla} G_\nu = \frac{\partial G_\nu}{\partial x_1} \vec{i} + \frac{\partial G_\nu}{\partial r_1} \vec{e}_r + \frac{i\nu}{r_1} G_\nu \vec{e}_\theta \quad (66)$$

G_ν is given by (62),

$$G_\nu(x_1,r_1;x_0,r_0,\theta_0)$$
$$= -\frac{\epsilon_0}{2\pi^2} \frac{1}{\sqrt{r_1 r_0}} e^{-i\nu\theta_0} Q_{\nu-1/2}(z) \quad (62)$$

with,

$$z = \frac{(x_1-x_0)^2 + r_1^2 + r_0^2}{2 r_1 r_0}$$

Refer to Figure 9 for notation. The derivatives in (66) are,

$$\frac{\partial G_\nu}{\partial x_1} = G'_\nu(z) \frac{\partial z}{\partial x_1}$$

$$\frac{\partial G_\nu}{\partial r_1} = G'_\nu(z) \frac{\partial z}{\partial r_1} - \frac{1}{2r_1} G_\nu(z)$$

where,

$$G'_\nu(z) = -\frac{\epsilon_0}{2\pi^2} \frac{1}{\sqrt{r_1 r_0}} e^{-i\nu\theta_0} Q'_{\nu-1/2}(z) \quad (67)$$

and

$$Q'_{\nu-1/2}(z) = \frac{\nu-\frac{1}{2}}{z^2-1} [z Q_{\nu-1/2}(z) - Q_{\nu-3/2}(z)] \quad (68)$$

Surface Integration

The double integrals, (59) and (65), must be evaluated over the hull surface. The integral for the potential, (59), will be explicitly considered in the following, but (65) can be handled identically.

Referring to Figure 9, (59) can be written,

$$\phi_{i\nu}(x_1,r_1) =$$

$$= \int_{x_0=-L_f}^{L_a} \int_{\alpha_0=0}^{2\pi} K_i(x_0,\alpha_0) G_\nu(x_1,r_1,x_0,\alpha_0) d\alpha_0 dx_0$$

$$(69)$$

where

$$K_i(x_0,\alpha_0) = \sigma_i(x_0,\alpha_0) \rho_0 \sqrt{1 + \left(\frac{1}{\rho_0}\frac{\partial\rho_0}{\partial\alpha_0}\right)^2 + \left(\frac{\partial\rho_0}{\partial x_0}\right)^2}$$

$$(70)$$

ρ_0 and α_0 are cylindrical coordinates in the hull system located at the intersection of the design waterline and the vertical centerplane. On the hull surface,

$$\rho_0 = \rho_0(x_0,\alpha_0)$$

For the hull system located in the same vertical plane with the propeller, the limits $-L_f$ and L_a on the x_0 integral in (69) correspond to the forward and aft ends of the hull waterplane, respectively.

Over the submerged surface of typical ship hulls the derivative $\partial\rho_0/\partial x_0$ in (70) will be small relative to 1, even near the ends. Therefore, (70) can be approximated by,

$$K_i(x_0,\alpha_0) \approx \sigma_i(x_0,\alpha_0) \rho_0 \sqrt{1 + \left(\frac{1}{\rho_0}\frac{\partial\rho_0}{\partial\alpha_0}\right)^2} \quad (71)$$

(69) then can be written,

$$\phi_{i\nu}(x_1,r_1) =$$

$$= \int_{x_0=-L_f}^{L_a} \int_{C(x_0)} \sigma_i(x_0,\ell) G_\nu(x_1,r_1;x_0,\ell) d\ell dx_0 \quad (72)$$

where, in (72) the inner line integral is around the hull section contour, $C(x_0)$, at the axial station x_0; ℓ is length along the contour, Figure 10.

The approximation, (71), allows the double integration in (72) to be conveniently performed. With $\partial\rho_0/\partial x_0$ discarded in (71) the contour integrals over the hull sections are independent of one another. This independence of the hull sections furthermore suggests a "strip-wise" determination of the source densities σ_i, which is consistent
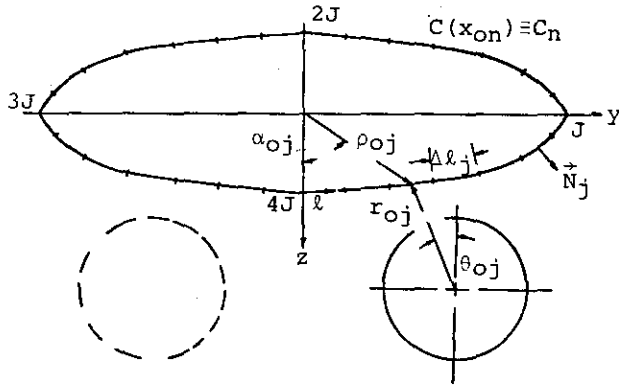
Figure 10. Hull Section Contour

with the "slenderness" assumption of (71). Determination of the σ_i will be considered further on.

Denote the contour integral in (72) as I^ν,

$$\phi_{i\nu}(x_1,r_1) = \int_{x_o=-L_f}^{L_a} I^\nu(x_1,r_1;x_o)dx_o \qquad (73)$$

(73) will be executed using some quadrature rule; the trapezoidal rule has been found to be convenient,

$$\phi_{i\nu}(x_1,r_1)=\frac{1}{2}\sum_{n=1}^{M-1}(I_{n+1}^\nu+I_n^\nu)(x_{on+1}-x_{on}) \qquad (74)$$

where $I_n^\nu=I^\nu(x_1,r_1;x_{on})$
M in (74) is the total number of axial stations over the ship length. Considering I_n^ν,

$$I_n^\nu= \int_{C_n} \sigma_{in}(\ell)G_\nu(x_1,r_1;x_{on},\ell)d\ell \qquad (75)$$

C_n denotes the contour of the hull section at station n.

Referring to Figure 10, the contour C_n is that of the "double-hull" by definition of $S^*(R_o)$ in (51). The contour is therefore doubly symmetric with respect to the waterplane and the vertical centerplane. Divide the contour into 4J segments each of length $\Delta\ell_j$, arranged with J segments per quadrant such that the double symmetry is retained in the segmented contour. Denoting r_{oj} and θ_{oj} as the coordinates to the midpoint of the jth segment in the propeller system, (75) can be evaluated approximately by the rectangle rule as,

$$I_n^\nu= \sum_{j=1}^{4J} \sigma_{inj} \, G_\nu(x_1,r_1;x_{on},r_{oj},\theta_{oj})\Delta\ell_j \qquad (76)$$

σ_{inj} is the source density at the midpoint of the jth segment.

In order to satisfy the condition of zero potential on the water surface, a negative image source density is required on the image hull. The hull surface forces of primary interest are the vertical and athwartship, i=3 and 2, respectively. For unit vertical velocity of the hull (i=3) the source density will be symmetric about the vertical centerplane; for unit athwartship velocity the source density will be asymmetric about the vertical centerplane. Exploiting these symmetry considerations, (76) can be written,

$$I_n^\nu = \sum_{j=1}^{J} \sigma_{inj}[G_\nu(x_1,r_1;x_{on},r_{oj},\theta_{oj})$$

$$- G_\nu(x_1,r_1;x_{on},r_{oJ+j},\theta_{oJ+j})$$

$$\mp G_\nu(x_1,r_1;x_{on},r_{o2J+j},\theta_{o2J+j}) \qquad (77)$$

$$\pm G_\nu(x_1,r_1;x_{on},r_{o3J+j},\theta_{o3J+j})]\Delta\ell_j$$

where for the $\pm$ in (77), the upper sign corresponds to vertical analysis and the lower sign corresponds to athwartship analysis. The G_ν in (77) is, from (62),

$$G_\nu(x_1,r_1;x_{on},r_{oj},\theta_{oj}) =$$

$$=-\frac{\epsilon_o}{2\pi^2}\frac{1}{\sqrt{r_o r_1}} e^{-i\nu\theta_{oj}}Q_{\nu-1/2}(z_{nj}) \qquad (78)$$

with

$$z_{nj} = \frac{(x_1-x_{on})^2+r_1^2+r_{oj}^2}{2r_1 r_{oj}}$$

(78), substituted into (77), along with the σ_{inj} on the 1/4-contour, with the result substituted into (74), gives the νth harmonic of the hull induced potential at propeller radius r_1. $x_1=\kappa r_1$ by (46).

The identical scheme can be used to evaluate the velocity, $\vec{v}_{i\nu}$, from (65); the G_ν in (77) are merely replaced by the $\vec{\nabla}G_\nu$ from (66), (67), and (68).

With regard to the actual computation, given the σ_{inj}, M in (74) will normally be on the order of 50 for convergent results, and J in (77) should seldom need be larger than 10. The 50 M stations should be concentrated in way of the propeller since $\phi_{i\nu}$ and $\vec{v}_{i\nu}$ require evaluation in the propeller plane. Distributions typical of that shown on Figure 11 have been used, although representation of the forebody is actually unnecessary.

With 50 axial stations and 10 segments per quadrant per axial station, around 2,000 G_ν evaluations are required for evaluating the potential harmonic at one propeller radius. For a maximum of 9 propeller radii used in the force calculation by (64), approximately 20,000
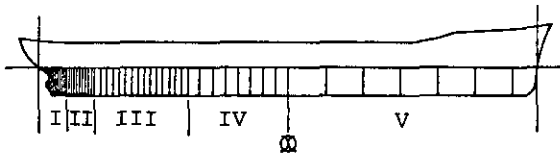
REGION	STATION DENSITY $\Delta x/L$
I	1/600
II	1/200
III	1/60
IV	1/30
V	1/15

Figure 11. Longitudinal Distribution
of Ship Stations

evaluations of (78) are required. For single-screw ships, the number of required $Q_{\nu-1/2}$ evaluations in (78) will be one-half of the above value since, with the symmetry, only two different z_{nj} are involved in (77).

Computation of Legendre Functions

The Legendre function of the second kind, of half-integer order, $Q_{\nu-1/2}(z)$, has the following series representations for small and large values of the argument z, [8],
For small $z \to 1$,

$$Q_{\nu-1/2}(z) =$$

$$\sum_{s=0}^{\infty} a_{\nu s}(z-1)^s + [\ln(z-1)] \sum_{s=0}^{\infty} b_{\nu s}(z-1)^s \quad (79)$$

with

$$b_{\nu s+1} = b_{\nu s} \frac{\nu^2 - \frac{1}{4} - 's(s+1)}{2(s+1)^2}$$

$$a_{\nu s+1} = a_{\nu s} \frac{\nu^2 - \frac{1}{4} - s(s+1)}{2(s+1)^2}$$

$$- b_{\nu s} \frac{2(\nu^2 - \frac{1}{4}) + (s+1)}{2(s+1)^3}$$

and

$$b_{\nu o} = -\frac{1}{2}$$

$$a_{\nu o} = \frac{5}{2} \ln 2 - 2 \sum_{j=1}^{\nu} \frac{1}{2j-1}$$

For large $z \gg 1$,

$$Q_{\nu-1/2}(z) = \frac{1}{2} \sum_{s=0}^{\infty} \frac{\Gamma^2(\nu+s+1/2)}{s!\,(2\nu+s)!} \left(\frac{2}{z+1}\right)^{\nu+s+1/2}$$

$$(80)$$

It has been found that the two above asymptotic forms can be overlapped to compute $Q_{\nu-1/2}(z)$ to three place

accuracy for $1 < z < \infty$ and for $\nu = 0$ to 11 with the number of terms in neither series, (79) or (80), exceeding 15.

Evaluation of Hull Surface Source Density

The underwater portion of a typical ship hull can be characterized as slender, implying that rates of change of surface geometry in the axial direction are small. For such a slender body in lateral motion the 3-dimensional source density, $\sigma_i(\vec{R}_o)$, required in (59) and (65) can be approximated by a an axial distribution of 2-dimensional "strip" source densities evaluated on hull section contours. This is consistent with the reduction of (69) to (72).

The one-dimensional integral equation which determines the source density on the hull contour at x_o is,

$$\vec{\alpha}_i \cdot \vec{N}(P) = \frac{\sigma_i(x_o, P)}{2} + \frac{1}{2\pi} \oint_{C(x_o)} \sigma_i(x_o, Q) \vec{N}(P) \cdot$$

$$\cdot \vec{\nabla} \ln(P,Q) \, d\ell \quad (81)$$

$\vec{N}$ is the contour outward normal, Figure 10. For $\vec{j}$ and $\vec{k}$ being unit vectors in the y and z directions, respectively, on Figure 10,

$$\vec{\alpha}_3 = \vec{k} \quad \text{for vertical analysis and}$$

$$\vec{\alpha}_2 = \begin{cases} \vec{j} & \text{on hull contour proper} \\ -\vec{j} & \text{on image hull contour} \end{cases}$$

for athwartship analysis. The P and Q in (81) denote "field point" and "source point," respectively, on the contour and (P,Q) denotes the Descartes distance between points P and Q on the contour.

Equation (81) can be solved for σ_i by representing the contour approximately by straight line segments, with the source density taken as a constant over each line segment. This is the approach employed by Frank, [9], for a 2-dimensional body oscillating in a free-surface, as well as by Hess and Smith, [10], for 3-dimensional infinite fluid problems, where patches of constant source density are used.

As explained in the development of (77), symmetry implies that the source density over only one quadrant of the complete contour of Figure 10 is unique; the source density distributions corresponding to the remaining three quadrants are positive and negative reflections of the first, the sign depending on the direction of motion (i=2 or 3).

Exploiting the symmetry conditions similarly to (77), (81) can be written as the system of J simultaneous equations,

$$\vec{\alpha}_i \cdot \vec{N}_j = \frac{\sigma_{inj}}{2} + \sum_{\substack{k=1 \\ k \neq j}}^{J} \sigma_{ink} H_{jk} \qquad j=1,J \qquad (82)$$

Here, the 1/4-contour has been segmented into J segments as shown on Figure 12. σ_{inj} in (82) corresponds to the constant source density of segment j on contour C_n, which is precisely the data required
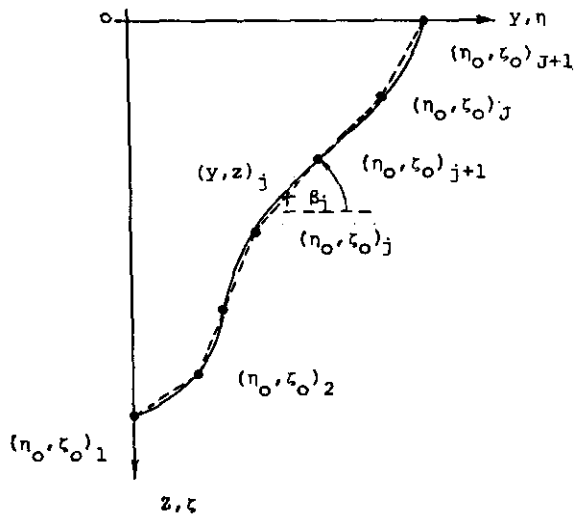

Figure 12. Contour Geometry

in the potential evaluation by (77). $\vec{N}_j$ is (82) is,

$$\vec{N}_j = \cos\beta_j \; k + \sin\beta_j \; j$$

where β_j is the slope of the j segment on Figure 12,

$$\cos\beta_j = \frac{\eta_{oj+1} - \eta_{oj}}{\Delta\ell_j}$$

$$\sin\beta_j = \frac{\zeta_{oj} - \zeta_{oj+1}}{\Delta\ell_j} \qquad (83)$$

$$\Delta\ell_j = \sqrt{(\eta_{oj+1} - \eta_{oj})^2 + (\zeta_{oj+1} - \zeta_{oj})^2}$$

H_{jk} in (82) is,

$$H_{jk} = C_{j,k} - C_{j,J+k} \mp C_{j,2J+k} \pm C_{j,3J+k}$$

where the upper sign corresponds to vertical analysis and the lower sign corresponds to athwartship analysis, just as in (77).

$$C_{jk} = \frac{1}{2\pi} \int_{-\Delta\ell_k/2}^{\Delta\ell_k/2} \vec{N}_j \cdot \vec{V}_j \; \ln \rho_j(\ell) d\ell \qquad (84)$$

with,

$$\rho_j(\ell) = \sqrt{(y_j - \eta)^2 + (z_j - \zeta)^2}$$

$\rho_j(\ell)$ being the distance between the midpoint of the jth segment and the point (η, ζ) on the kth segment. The gradient is taken with respect to (y_j, z_j).

(84) can be integrated exactly. The integration is most readily accomplished in a coordinate system located in the kth element as shown on Figure 13. Write C_{jk} as

$$C_{jk} = \vec{N}_j \cdot \vec{v}_{jk} \qquad (85)$$

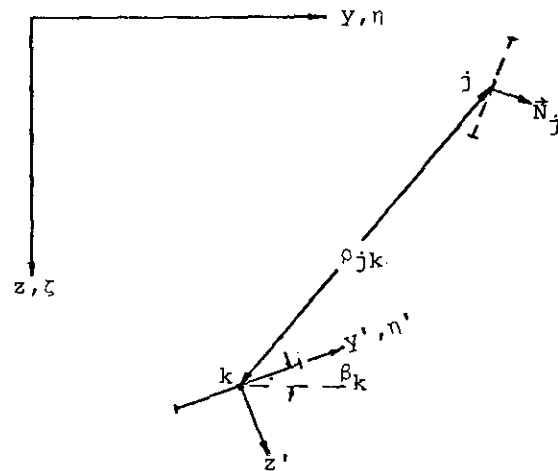where $\vec{v}_{jk}$ is the velocity induced at the

Figure 13. Contour Coordinate Systems

midpoint of the jth element by the kth element. Write $\vec{v}_{jk}$ as,

$$\vec{v}_{jk} = w_{jk} \; \vec{k} + v_{jk} \; \vec{j}$$

with

$$w_{jk} = w'_{jk}\cos\beta_k - v'_{jk}\sin\beta_k$$

$$v_{jk} = w'_{jk}\sin\beta_k + v'_{jk}\cos\beta_k \qquad (86)$$

w'_{jk} and v'_{jk} are the velocity components at j in the local coordinate system of k, Figure 13; β_k is given by (83).

In the local system,

$$w' = \frac{\partial\phi'}{\partial z'}, \qquad v' = \frac{\partial\phi'}{\partial y'}$$

where,

$$\phi'_{jk} = \frac{1}{2\pi} \int_{\eta'=-\Delta\ell_k/2}^{\Delta\ell_k/2} \ln\sqrt{(y_j'-\eta')^2 + z'_j{}^2} \; d\eta'$$

and,

$$y_j' = \frac{y_i - y_k}{\cos\beta_k}, \qquad z'_j = \frac{z_j - z_k}{\cos\beta_k}$$

Then, by exact integration,

$$w'_{jk} = \frac{1}{2\pi} \left[\text{sgn}(\eta'-y'_j)\,\text{sgn}(z'_j)\tan^{-1}\frac{|y'_j-\eta|}{|z'_j|} \right]_{\eta'=-\Delta\ell_k/2}^{\Delta\ell_k/2}$$

(87)

and

$$v'_{jk} = -\frac{1}{4\pi}\ln[(y'_j-\eta')^2+z'^2_j]\Big|_{\eta'=-\Delta\ell_k/2}^{\Delta\ell_k/2}$$

If the distance between elements is sufficiently large $\rho_j(\ell)$ can be approximated by $\rho_{jk}=\sqrt{(y_j-y_k)^2+(z_j-z_k)^2}$ so that (84) becomes,

$$C_{jk} = \frac{1}{2\pi}\vec{N}_j\cdot\vec{V}_j\,\ln\rho_{jk}\Delta\ell_k$$

(88)

Use of (88) is equivalent to placing a point source of strength $Q=\sigma_{ink}\Delta\ell_k$ at the midpoint of the kth line segment, or simply evaluating the integral (81), in terms of the unknown σ_{in}, by the rectangle rule.

It has been found that (88) should not be used when $\rho_{jk}<2.5\Delta\ell_k$; for elements in close proximity the exact integration by way of (85), (86), and (87) should be used.

(82) represents a system of J simultaneous linear equations in J unknown σ_{inj}. This system must be solved for n=1 to M stations along the hull. For J=10 and M=50 as proposed in the discussion of (77) and (78), the approximation to the complete hull surface source density required in computing the hull induced potential by (74) therefore requires solving 50 independent sets of 10x10 systems of simultaneous linear equations.